Fall 2017

Experimental and numerical study on failure strength of aspirated cell membrane

Yang Wu
University of Iowa

EXPERIMENTAL AND NUMERICAL STUDY ON FAILURE STRENGTH OF ASPIRATED CELL MEMBRANE

by

Yang Wu

A thesis submitted in partial fulfillment
of the requirements for the Master of Science
degree in Mechanical Engineering in the
Graduate College of
The University of Iowa

December 2017

Thesis Supervisors: Professor Sarah C. Vigmostad
Professor Jia Lu

Graduate College
The University of Iowa
Iowa City, Iowa

CERTIFICATE OF APPROVAL

_____

MASTER'S THESIS

_____

This is to certify that the Master's thesis of

Yang Wu

has been approved by the Examining Committee for
the thesis requirement for the Master of Science degree
in Mechanical Engineering at the December 2017 graduation.

Thesis Committee: _____
Sarah C. Vigmostad, Thesis Supervisor

_____
Jia Lu, Thesis Supervisor

_____
Michael D. Henry

To Vigmostad and Lu for their advice with profession and experience, encourage and support.

To Chen and my family for all the love and their unending support, inspire and care.

Don’t worry about failures, worry about the chances you miss when you don’t even try.

Jack Canfield
Chicken Soup for the Soul

ACKNOWLEDGEMENTS

This master thesis marks the end of my two-year journey in Iowa City. I would like to take this opportunity to thank both of my academic advisors and mentors Dr. Sarah Vigmostad and Dr. Jia Lu. I couldn't have completed my research without their great support and guidance. Their influence to me is not restricted to the area of my study but the dialectical attitude of research, acceptance of different ideas and dedication to meaningful work. Dr. Vigmostad shared her expertise in Cellular Biomechanics, discovered my interest provided with best equipment and resources possible. Dr. Lu presented a strong knowledge of mechanics and inverse study and influenced me through effective guidance on developing quantification method.

I would also like to take this opportunity to thank my research colleague Krog Benjamin from Dr. Michael Henry's Biophysics Lab. Ben was the one who taught me every detail about the experiment I performed, answered all the questions I had related to cellular behavior under the microscope and prepared and cultured all the cells for me.

With no doubt, I would also like to thank my family for their continuous support and encouragement throughout my study life. Thank my father for 'sowing the seed' that inspired me to study abroad in the United States. Thank my mother who has always motivated me to strive for a better life. Thank my grandparents for accompanying with me throughout my childhood, taught me right and wrong, guided me comprehended the meaning of life. Lastly, I would like to express my deepest gratitude to my girlfriend for her tolerance, belief, support, and sacrifice for the past three years, accompanied by me and shared beautiful days together.

ABSTRACT

The objective of this work is to develop an innovative and quantitative method to study cell failure under fluidic pressure to understand cell membrane mechanical properties. Due to lack of experimental data related to cell failure property, the current research focuses on investigating the cell failure using a micro pipette aspiration experiment method to elaborate gradually increasing hydrostatic pressure to the cell causing the membrane to deform and eventually rupture. Based on our observation, the prostate cancer cells (PC-3) deformed into a deflated and flattened shape under higher hydrostatic pressure (249 Pa) while prostate epithelial cells (PrEC LH) cells generate a spherical and rounded shape. The stress along the cell membrane was estimated from the curvature data captured from the 2D microscopic images for each pressure magnitude to quantify the damage before rupture state. From the results, non-transformed prostate epithelial cells (PrEC LH) presented a stiffer and rupture resilient property compared to transformed prostate cancer cells (PC-3) which presented a softer and vulnerable property. Besides, the alteration of shape of the aspirated membrane directly affected the stress distribution over the membrane and as a result, provoked membrane failure. Multiple pieces of research have shown a higher stiffness of healthy cells compared to cancer cells including one of the previous studies done by our group which have also found that cancer cell tends to become stiffer after exposing to fluid shear stress. The discovery of this cellular behavior and novel numerical quantification method of cell failure could advance the study of cancer cell membrane failure, cellular matrix structure, response to mechanical loadings and potentially foundation in developing new treatment for cancer other than destructive chemical treatment.

PUBLIC ABSTRACT

Cancer, which was responsible for 595,690 cases of death in 2016 according to national statistics, has surpassed heart disease and became the most severe cause of death in the United States. Among all cancer related cases, 90% cancer death was due to cancer cell metastasis which is caused by transformed cancer cells reproduced from the primary tumor, travel and relocate causing destructive damage to vital organs in that area. To develop an in-depth understanding of failure property, the current research uses a micropipette aspiration system to elaborate hydrostatic pressure to the cell causing the membrane to deform and eventually rupture. Based on our observation, the prostate cancer cells (PC-3) deformed into a deflated and flattened shape under higher hydrostatic pressure while prostate epithelial cells (PrEC LH) cells generate a spherical and rounded shape. By analyzing stress data generated from processed microscopic images, our study shows that cancer cells may be not only softer than healthy cells but also more susceptible to rupture. The alteration of shape of the aspirated membrane directly affected the stress distribution over the membrane and as a result, provoked membrane failure. Multiple pieces of research have shown a higher stiffness of healthy cells compared to cancer cells including one of the previous studies done by our group which have also found that cancer cell tends to become stiffer after exposing to fluid shear stress. The discovery of this cellular behavior and novel numerical quantification method of cell failure could advance the study of cancer cell membrane failure, cellular matrix structure, response to mechanical loadings and potentially foundation in developing new treatment for cancer other than destructive chemical treatment.

TABLE OF CONTENTS

LIST OF FIGURES

CHAPTER 1: INTRODUCTION

1.1 BACKGROUND

Cancer remains as one of the deadliest diseases in the world. According to a national incident and mortality statistics conducted in 2016, 1,685,210 new cancer cases were leading to 595,690 cancer deaths occurred in the United States which is currently the leading cause of death in 21 states (Siegel, Miller, & Jemal, 2016). Cancer is deadly primarily due to its migratory property which originates from abnormal cancer cells that reproduce themselves, migrate distant from the primary tumor through the blood and lymphatic vessels and attach to varied tissue environments called cancer cell metastasis (Suresh, 2007). Multiple research articles have indicated that over 90% cancer death cases were due to cancer cell metastasis from solid tumors (Gupta & Massagué, 2006; Mehlen & Puisieux, 2006; Wirtz, Konstantopoulos, & Searson, 2011). Despite the high death rate of cancer cell metastasis, the metastatic process is highly inefficient that few cells can successfully migrate to distant sites due to apoptosis. The inhibition of cell death was emphasized by Mehlen and Puisieux (2006) as a critical characteristic of metastatic cancer cells. Important parameters throughout cell metastasis have caused cell apoptosis while cancer cells adapted and react to survive the process. A primary hypothesis is that the immune system and hemodynamic forces could be responsible for the cell death during metastasis (Luzzi et al., 1998). While there were extensive research and progress on immune system regulating cell apoptosis, rarely has the effect of physical interaction within microvasculature including hemodynamic parameters been studied or experimentally

proved by researchers. One of the studies suggested that cells under metastasis in the microvasculature could be potentially damaged by friction or adhesion between individual cancer cells and capillary walls. Also, hemodynamic destruction may be an equally important underestimated cause of metastatic inefficiency (Weiss, Dimitrov, & Angelova, 1985). For the past decade, biologists have put tremendous effort and developed multiple quantification methods in studying biomechanical and biophysical properties of cells and subcellular structures. To better understand the cell biomechanics relating to cancer cell metastasis, it is important to study cell deformability and elasticity as they affect cellular mechanotransduction, morphology, signaling, and migration (Hochmuth, 2000). The ability to quantify material properties of cells and its response to mechanical stimuli could provide significant insight into the investigation of how cancer cells survived hemodynamic destruction. Cancer cells have different deformability and elasticity, many researchers have reported that cancer cells have altered cytoskeleton and extracellular matrix structure comparing to healthy cells which influence the size, shape, and stiffness (Suresh, 2007). One of our recent findings even indicates that cancer cells may stiffen themselves as a response to experiencing high fluid shear stress while healthy cells do not have the similar response (Chivukula, Krog, Nauseef, Henry, & Vigmostad, 2015). We are curious to know how the change of the material property would affect their rupture rate and failure strength under mechanical loading. In fact, little is known or reported by researchers about the failure strength of cell membrane either for cancer or healthy cells. This leads us to follow up with a set of micro pipette aspiration experiments and numerical study on

determining how cells react to destructive mechanical loading, and to quantify the pressure-induced stress in the cell membrane.

1.2 MICROPIPETTE ASPIRATION

A micro pipette aspiration system is developed to study mechanical properties of living cells by aspirating cells into a finely constructed micropipette, causing cell membrane inside the transparent tube to deform. To produce accurate and consistent results, the system usually contains a pressure transducer to control the pressure applied to the aspirated cell. Besides, a micro manipulator is essential to guide the micropipette to the target cell and keep the cell in suspension during the process. This method outperforms other techniques for several reasons: First, the cell needs to be examined in a suspended form to retain its original shape and reduce the abrasion against the cover slip substrate, as mentioned earlier that cells tend to stiffen themselves when they are in a fixed state. Second, the aspiration power is easily controlled by a pressure transducer so that we could examine the deformation of the inner cell membrane in equilibrium at different pressure gradients. Moreover, if necessary, micro pipette aspiration could load significant force to deform cell membranes to their rupture point, rarely have researchers reported any force or stress measurement for cell damage or yielding stress so our results can be innovative to cancer diagnosis and treatment.

1.3 CHARACTERIZATION OF CELLS

In general, the elastic modulus is a key property to characterize deformable materials. With the multiple steps of pressure load applied and transferred to the

micropipette, the cell will be aspirated onto the tip of the micropipette, and then slowly aspirated into the micropipette tube. The change of shape inside the tube can be seen through the transparent pipette. Inner projection length of the aspirated membrane is defined as L_p, the inner radius of the pipette tube is defined as R_p, the radius of the cell is defined as R_c, ΔP is the pressure difference between the inner cell and outer environment inside the micropipette which will be referred as suction pressure later. A schematic view of cell aspirated into a pipette is shown in Figure 1.

Cell behavior under micro pipette suction can be divided into solid and fluid type. Generally, both types behave similarly until hydrostatic pressure aspirates the membrane and forms a hemispherical projection inside the pipette. As the aspirated behavior is largely dependent on the pipette diameter, a standard ratio of projection length and radius of the micropipette, L_p/R_p = 1 is often used to differ solid and liquid cell types. The soft cells such as neutrophils and red cells which flow freely into the pipette when the pressure increased beyond the standard L_p/R_p = 1 are defined as liquid type cells. On the contrary, rigid cells such as chondrocytes and endothelial cells, which reform its shape and reach equilibrium inside the pipette again when the pressure increased beyond the standard L_p/R_p = 1 are defined as solid type cells with an elastic modulus of 500 $pN/\mu m^2$(0.5kPa) (Hochmuth, 2000). A schematic view of the difference between liquid type cell and solid type cell is shown in Figure 2.

1.4 EXISTING CHARACTERIZATION TECHNIQUES

Among sparse of experiment methods providing measurements to investigate mechanical properties for cells including Atomic Force Microscopy, Optical Tweezers, Microfluidic deformability cytometry and Micropipette Aspiration, Micropipette aspiration was particularly used for investigating mechanical properties of cancer cells in this study due to its simplicity, versatility and the ability to allow cells studied in suspension state since most cells are suspended during metastasis. A brief introduction to those existing techniques is provided below:

Optical trap: The optical trap, also named as optical stretcher consisted beam laser traps to stretch suspended target cell causing deformation and measure optical deformability and surface force generated(Guck et al., 2005). One of the greatest advantages of this method is that cells are measured in suspension so that the environment is similar to its original state in circulation. Also, the system is developed with excellent control that could provide a broad range of loading conditions including attractive or repulsive force. A more developed modified dual-beam laser trap called optical cell rotator was developed for holding and rotating micro dielectric particles including cells(Kreysing et al., 2008) which enable 3D cell structure studies in the future. On the other hand, the uncertainty remains as the higher light intensities required for important force scale measurement could potentially provide untold damage to the cells.

Atomic force microscopy (AFM): Atomic force microscopy functions as using a sharp tip scanning over the material surface at a constant velocity, creating a 3D force versus indentation plot. The force difference required for causing an indentation on the cell

membrane surface provides the stiffness of the material. Most studies that have successfully applied this method to investigate living cells limited the loading within 10 nN (Lekka et al., 1999). While Atomic force microscopy is significant in determining the surface texture and structure, our particular focus of cell membrane's failure stress has derived us from this method. Some other literature also mentioned that AFM is inaccurate when measuring small scale forces (10-15pN) due to thermal fluctuations and inconsistent force-deformation relationship when switching between varies shape of AFM probe.(Hochmuth, 2000) Furthermore, studies have reported that cell tends to stiffen themselves up to 20-50 times when they are in a fixed state attached to the glass cover substrate, and they cannot reach its rupture point with the indentation(Lulevich, Zink, Chen, Liu, & Liu, 2006). Although some studies have argued that the result is consistent when mapping over the same cell multiple times proving the cell is undamaged through the process, AFM indisputable remains as one of the methods that could damage the cell and result in the measurement of a dead cell.

Microfluidic Deformability Cytometry: The microfluidic deformability cytometry method delivers cells stream to a stretching extensional flow to deform the cell at high strain rates and capture the data by a high-speed camera. This method is particularly useful in studying large group of cells by computational analysis and extract quantitative parameters from massive data distribution (Gossett et al., 2012) Although the system is able to process approximately 2000 cells/s, the result is very inaccurate and the force measurement is in dynamic state and hard to measure the exact force applied.

1.5 OBJECTIVES OF THIS STUDY

To explain cell metastasis inefficiency and decrease the cancer death rate caused by cancer metastasis, our group devoted ourselves to the understanding of cell biomechanics including elasticity, deformability, and rupture strength.

Previously, Barnes team discovered that cancer cells were less likely influenced by hemodynamic shear force while non-cancer cells were more susceptible to the damage due to several oncogenes which can potentially contribute to hematogenous metastasis(Barnes, Nauseef, & Henry, 2012). Also, a recent study carried by Chivukula had further proved this unique property of cancer cell. From the experiment, he observed that transformed prostate cancer cells (PC-3) appear to stiffen themselves upon exposure to fluid shear stress and the stiffening level increase based on the magnitude of fluid shear stress exposure. In contrast, non-transformed prostate epithelial cells (PrEC LH) do not change its material property when exposing to fluid shear stress. This phenomenon that appears only on cancer cells sheds new light on the cancer cells behavior during metastasis(Chivukula et al., 2015).

Most researchers and studies have focused on studying Young's modulus of the cell, rarely have studies reported the failure strength – the maximum tension in the cell membrane at which the cell ruptures. This is a critical property relevant to materials resistance to failure. The current research is primarily focusing on developing a quantitative method to track the localized membrane surface and calculate stress along the cell membrane when the cell is gradually aspirated by micro pipette until the hemispherical membrane projection inside the pipette develops a local bleb indicating a material failure. As our focus is still targeting cancer cells during metastasis which are cells in suspension,

an experiment method is necessary to provide enough loading until cell gets to rupture point while not sacrificing accuracy. Micropipette aspiration technique is still the best suit compare to other methods including atomic force microscopy and optical tweezers. Figure 3 shows a set of microscopic figures when cells are aspirated into micropipette tube under different pressure level and we could observe the change of the membrane through the transparent tube. Part of the cell membrane which is located inside the micropipette tube was modeled using a computational model, a spline curve that interpolates the membrane shape. The tension in the cell membrane is then estimated using an axisymmetric model. By studying the difference between cell membranes' shape and the tension distribution, it could determine the strength of the different type of cells.

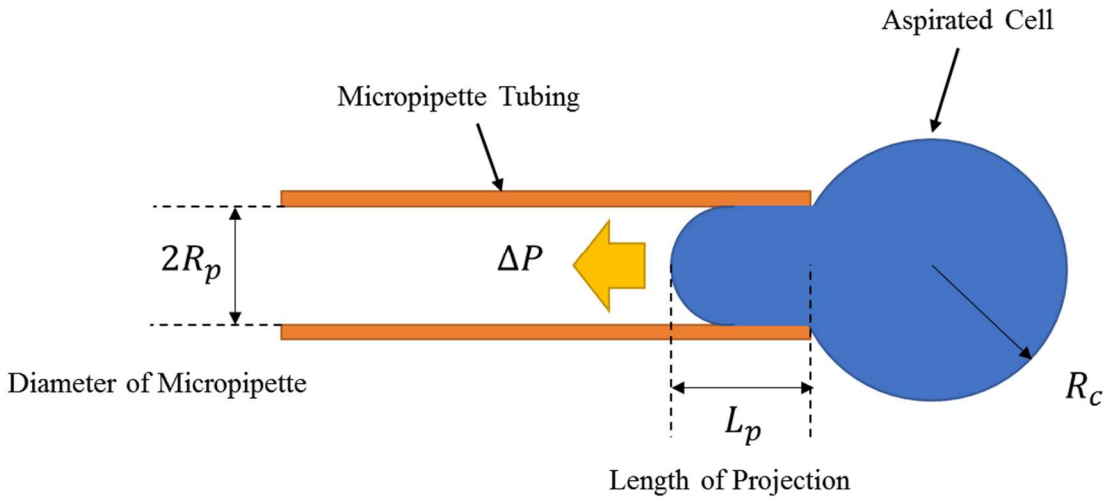

Figure 1: A schematic view of what micro pipette aspiration data images represent and what parameters are indicated. L_p represents the projection length inside the pipette and $R_p$represents the inner radius of the pipette. ΔP is the pressure difference between the inner cell and outer environment inside the micropipette.

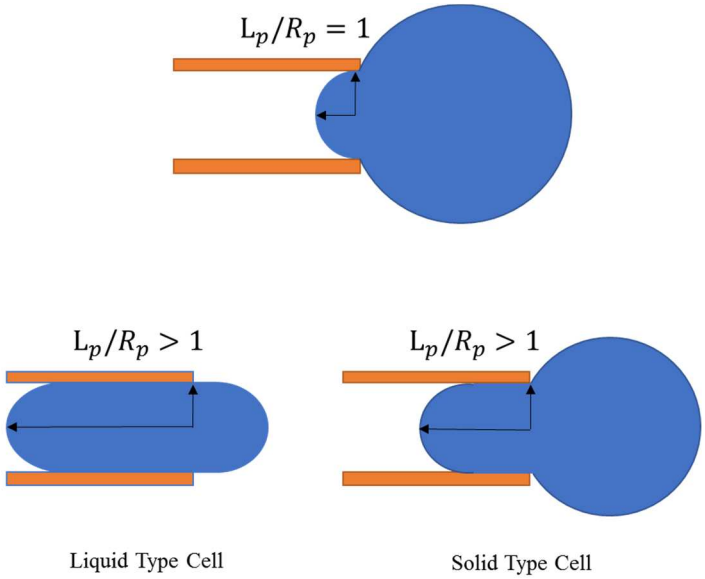

Figure 2: A schematic view of an aspirated cell into a pipette when Lp/Rp = 1, this is used to differ a solid type of cell and a liquid kind of cell. When Lp/Rp is larger than 1, if the cell membrane remains its position and achieves force equilibrium, the cell is considered solid type. However, if the cell flows freely into the micropipette, the cell is seen as liquid type.

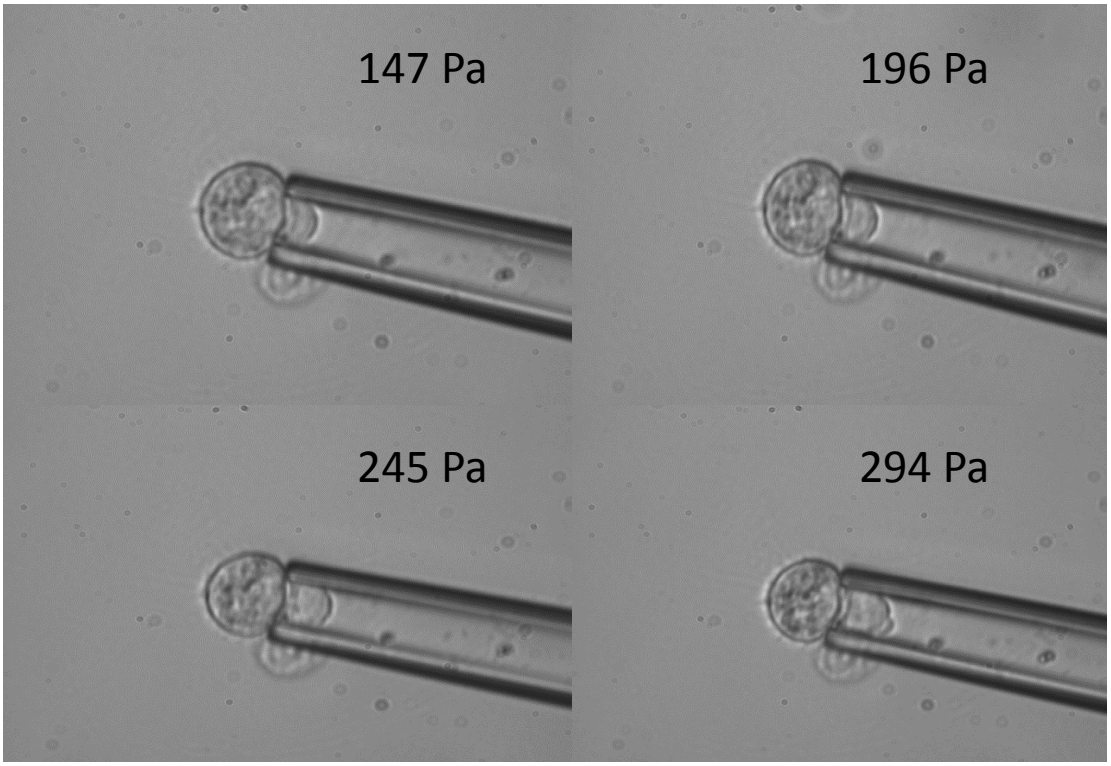

Figure 3 An example of a typical cell micro pipette aspiration image data set; the pressure level illustrated in Pascal. As the pressure increase, hydrostatic pressure cause cell aspirated into a micropipette and formed elongated projection inside micropipette. Eventually, the top of the membrane formed a local deformation, and we claimed this material failure to be ruptured.

CHAPTER 2: METHODS AND EXPERIMENTAL SETUP

2.1 EXPERIMENTAL INSTRUCTIONS AND TOOLS

The whole experiment could separate into two parts including pipette forge and cell aspiration. Comparing to pre-pulled pipettes available in the market, freshly pulled pipettes reveal less contamination from various possible sources which could potentially harm the experiment results. For the accuracy purpose, all the pipettes conducted in this experiment are freshly pulled. Pipette reproducing procedure consists of a micropipette puller (Figure 4), a micro forge (Figure 7) to fabricate thin-wall borosilicate capillaries into micropipette with high precision tips according to pipette cook book provided from Sutter Instrument. The aspiration experiment is necessary to be conducted in a room with minimum airflow and vibration. The system involves a micromanipulator (Figure 6) to control the movement of the pipette tip, a microscope (Figure 5) with a shockproof desk to avoid vibration during the experiment, a pressure regulator to control the water level and a camera to capture source images.

2.1.1 Micropipette Puller

A micro pipette puller (Model P-30, Sutter Instrument Co., Novato, CA, USA) is used to pull thin-walled, non-filament borosilicate capillary glass to form long, gently tapering tip. Borosilicate glass has the advantage of high strength, stiffness and ability to form smaller tips. Several parameter settings including temperature and break point are required for drawing the different type of pipettes are obtained from the Sutter pipette cookbook (Oesterle, 2015).The pulled capillaries then kept in a dust-free container to

prevent contamination until it needs to be forged with precision right before the experiment, preferably within a week.

2.1.2 Micro Forge

The micro forge (Narishige MF-900, Narishige Group, Tokyo, Japan) is used to finalize the micropipette crafting after pulled and broke the micropipette precisely at the desired diameter without any crack or length inconsistency. In general, micropipette pulled from the puller does not provide precise control over the tip diameter. Micro forge has a ruler mounted inside the eyepiece that could measure the exact diameter at the break location. Before forging, a glass bead needs to be forged around the heating wire using the same material as the capillaries (Borosilicate in this case) to expand forging capability.

2.1.3 Pressure Regulator

Pressure is regulated with a syringe with distilled water inside. By increasing or decreasing the water level aligns to the microscopic stage, it generates hydrostatic pressure to aspirate the cell through micropipette. After the pressure is calibrated, the reservoir represents the non-pressure state, and by controlling the micrometer screw pitch gauge on the side, the pressure level was adjusted according to the height of reservoir.

2.1.4 Micromanipulator

A micro manipulator (Scientifica LBM-7, Scientifica, Sussex, UK) is used to control the micropipette motion. It contains four linear and three rotational axes which allows a broad range of movement of pipette while maintaining high stability.

2.1.5 Microscope

The inverted microscope (Nikon TE-300, Nikon Corporation, Tokyo, Japan) provided with unhindered access to the cell sample on the slide rather than the traditional ones where cell samples are isolated. This microscope also capable of fluorescence microscopy so that it explores much more such as using an array of fluorochromes to identify cells, cell components and determining structural parameters of the cytoskeleton (Lichtenstein N, July 2003).

2.1.6 Camera

The Stingray camera (Stingray, Allied Vision Technologies GmbH, Stadtroda, Germany) is implemented on the side of the microscope. The software integrated with the camera record the aspiration process. The user can pause between the frame and search for the photo with the best focus on the target. Proper light adjustment and bright background significantly improve the result of the image that reduces the challenge of post image processing.

2.2 EXPERIMENT SETUP AND PREPARATION

Before operation sets up, thin borosilicate capillary glass was pulled using the micro pipette puller to form a long, gently-tapering pipette where the tip needs to be clean without any contamination. The capillary was clamped on both sides through a heating ring at the middle. After setting up the heating temperature and location were to provide capillary a hard pull according to the parameter from the cook book (Oesterle, 2015), heat ring melts the glass capillary, and it started to elongate until it eventually broke at the hard pull point.

Ideally, we could obtain two preliminary pipettes with long tapered tip drew out 10-15 mm. Examine both tips under the microscope since tip diameter needs to be less than the width we desire to break later and pipettes were carefully stored and transferred in a dust free environment.

To set up the experiment, the preliminary pipette was secured onto an extension probe. For each different capillary material, we used the capillary to melt and forge a glass bead around the heating wire for breaking purpose. During the breaking motion, preliminary micropipette tip is gently placed on the bead without causing any bending on the pipette. As the bead heated up, the tip would start to bend, and part of the pipette in contact with the bead will melt rapidly. To perform a clean edge at the tip, it is essential to adjust the micropipette to the longitudinal direction right after the heater was turned off as the temperature just drop down from the melting point. This method performed better than just withdraw the pipette backward to cause the break. Holding pipette (smaller diameter at the tip) can be forged by placing tip close to the glass bead and briefly heat the tip without touching it.

To connect pipette to the pressure regulator, micropipette was needed to fill with Phosphate-buffered saline (PBS) using a nonmetallic MicroFil syringe needle which was constructed from a combination of plastic and fused silica (World Precision Instruments, 2016). PBS filled micro pipette is connected with the pressure regulator used to control the inject and extract of aspiration. The connected micropipette was mounted to the micromanipulator pointing microscope stage at roughly 45-degree angle.

2.3 TYPE OF CELLS USED

In this study, transformed prostate cancer cells (PC-3) and immortalized, non-transformed prostate epithelial cells (PrEC LH) were used to perform micro pipette aspiration experiment. We will be referring all the prostate cancer cells as PC-3 cells and prostate epithelial cells PrEC cells in this article. This cancer line was obtained from American Type Culture Collection (Manassas, VA, USA) and cultured as recommended. Samples were collected at approximately 75-80% confluency with 0.25% trypsin. Cells were then suspended in DMEM/F12 medium containing 10% FBS to neutralize trypsin. Samples were centrifuged at room temperature for 5 minutes at 150g. Pellets were suspended to 5*10^5 cells/mL in DMEM medium. More details are given in (J.M.Barnes, J.T.Nauseef, & M.D.Henry, 2012).

2.4 EXPERIMENT PROCEDURE

The micropipette was adjusted extremely close the slide and microscope were adjusted until the micropipette tip can be fully observed. To calibrate the pressure regulator, a drop of PBS with 2% of polyethylene beads on the slide is used to keep the flow through the micropipette tip. After the micropipette was calibrated so that no beads were traveling in to or out of the micropipette, a drop of medium with the cell was deposit onto the slide. By using the micromanipulator, micropipette was navigated to the bottom of the medium where abundant cells were clinging on to the slide. By lowering the reservoir, a small suction pressure was used to pick up the cell and raised it into a suspended state. The reservoir was then lowered step by step, and the micropipette aspirates the cell gradually until the cell membrane eventually lost coherence and developed a localized deformation.

For each step, the height change of the reservoir was recorded as well as the image captured the final stage of micro pipette aspiration at that pressure level.

2.5 POST IMAGE PROCESSING

After the experiment, image data were transferred and imported into MATLAB and ImageJ for further processing to enhance contrast, edge detection. The essential goal was to extract the entire cell boundary outside and inside the pipette to study the shape change of membrane before and after localized deformation under incremental pressure. Keeping process standard identical for each set of cell data is essential to avoid manual tracing tolerance and improve the reliability of validation. A developed protocol is necessary for analyzing cell. Ideally, a computational algorithm with proper validation could eliminate human error.

2.6 CURVATURE STUDY

The current method of tracking cell boundary is to mark cell membrane boundaries with discrete points in Image J and then generate a 4^{th} order polynomial curve. The curve is compared to canny edge detector results to ensure it represents the membrane well.

Canny edge detection starts with smoothing the image with a Gaussian filter to eliminate subtle detail that could hardly consider as an edge. Upon detecting all the small edge fractions, it computes the edge strength and uses two thresholds to decide whether to connect edge pieces or discard it. The Canny algorithm has the advantage of adjustable parameters to fit for different scenario compared to other edge detectors available in

MATLAB such as Sobel and Prewitt, especially when the image is suffered from noise (Shrivakshan, 2012).This advantage allows adaptive edge detection to depend on the quality of the camera and noise caused by vibration at the moment when the photo is captured.

The stress function we used in this study relies on several assumptions. First, the cell membrane is assumed to bear in-plane stress only, no bending moment is considered. This treatment is consistent with most previous cell membrane analysis provided by Evans and his colleagues that bending modulus was negligible (Evans, Skarlek, & Weinbaumu, 1980). Second, the deformation of the cell membrane is considered to be axisymmetric so that only half of the convex curve is studied. This implies that the top of the cell membrane is flat with slope equal to zero. Also, at the top of the dome, the two principal stresses should always equal to each other. Third, the suction pressure ΔP is given by the displacement downward of the water reservoir controlled by the syringe.

$$\Delta P = \rho g \Delta h$$

In Hochmuth's review of previous work (2000), he mentioned that the minimum suction pressure is 0.1-0.2 pN/μm^2, limited by the fluctuations of the system and water evaporation, maximum suction pressure is 96 nN/μm^2, limited by the vapor pressure of water at room temperature. The force applied to the cell inside a micropipette under equilibrium is given as:

$$\mathrm{F} = \Delta \mathrm{P} \pi R_p^2$$

where ΔP is the suction pressure and R_p is the radius of the inner diameter of the pipette. While our focus of this study is solid type cell which has a shear rigidity to avoid flowing

into the pipette freely and cell generally reach their rupture point when $L_p \geq R_p$, an equation provided by Evan(1980) in his book described the relation between the suction pressure and the shear elastic modulus of the membrane

$$\Delta P = \left(\frac{\mu}{R_p}\right)\left[\left(\frac{2L_p}{R_p} - 1\right) + \ln\left(\frac{2L_p}{R_p}\right)\right] (L_p \geq R_p)$$

where μ is the shear elastic modulus of the membrane, Lp is the length of projection and Rp is the radius of the micropipette. Another analysis provided an infinite, homogeneous half-space drawn into a micropipette expression of Young's Modulus

$$\Delta P = \frac{2\pi}{3} E \frac{L_p}{R_p} \phi$$

where ΔP is the suction pressure, E is the Young's Modulus for the homogeneous solid and ϕ is a term depends weakly on the ratio of the thickness of the pipette wall to the radius of the pipette with a typical value of $\phi \approx 2.1$ (Theret, Levesque, Sato, Nerem, & Wheeler, 1988). From the previous studies of Chivukula (2014), both transformed prostate cancer cells (PC-3) and immortalized epithelial cells (PrEC LH) behaved as solid cells. The study uses the half space model developed by Theret to describe the relationship (D.P. Theret, 1988)

$$E = \frac{3a\Delta p}{2\pi L} \phi(\eta)$$

where E is the Young's Modulus for the homogeneous solid, ϕ depends on the ratio of the pipette wall to the radius of the pipette.

The target of our interest consists only the tip of the aspirated membrane which is referred as a hemispherical cap in the schematic diagram shown in Figure 8. Only the

right half of the membrane is modeled under axisymmetric assumption. Multiple discrete points were used to mark the boundary of the membrane on the source image, an example is shown in Figure 9. When tracing the curvature of the aspirated membrane, the polynomial curve is described by two polynomial functions which are controlled by two sets of polynomial coefficients p_a, p_b and curve length s, b is the break.

$$x = f(s) = p_a(s-b)^3 + p_a(s-b)^2 + p_a(s-b) + p_a$$

$$y = f(s) = p_b(s-b)^3 + p_b(s-b)^2 + p_b(s-b) + p_b$$

The original blurry boundary is replaced by a single curve described from two polynomial functions. The fitting quality can be justified by overlapping the original image with the fitted curve shown in Figure 10. The two polynomial functions are taken first and the second derivative to compute curvature function $k_1$on the meridional direction and k_2 on the circumferential direction.

$$k_1 = \frac{x'y'' - y'x''}{(x'^2 + y'^2)^{3/2}} \quad ; \quad k_2 = \frac{\sin(\arctan(\left|\frac{y'}{x'}\right|))}{r}$$

Where r is the horizontal distance from the center to the membrane, obtained from the absolute value of x. A schematic view of the tip of the membrane with the curvature directions labeled is shown in Figure 11. The curvature value k_1 and k_2 are used to calculate principal stress T_1 and T_2 using the Laplace Law.

$$T_1 = \frac{\Delta P}{2 \times k2} \quad ; \quad T_2 = \frac{\Delta P}{k2} \times (1 - \frac{k1}{2 \times k2})$$

Here ΔP is obtained from the hydrostatic pressure developed by the water level difference controlled by the syringe within the pressure regulator. For example, when water level difference is 15mm, the hydrostatic pressure caused by water level difference transferring

into the micropipette is equal to 147 Pa. Von Mises stress is calculated from the principle stresses T_1 and T_2.

$$Von\ Mises\ stress = \sqrt{{T_1}^2 + T_2^2 - T_1 \times T_2}$$

According to the Laplace Law, at an optimum state where the curvature is consistent throughout the curve, the stress is also consistent. The curvature analysis process diagram is shown in Figure 12, demonstrating a flowing process of analysis taken on a PrEC cell for Case 49.

Figure 4: Micropipette puller (Model P-30, Sutter Instruments, Novato, CA, USA)

Figure 5: Microscope (NikonTE-300, Nikon Corporation, Tokyo, Japan)

Figure 6: Micromanipulator (Scientifica LBM-7, Scientifica, Sussex, UK)

Figure 7: Microforge (Narishige MF-900, Narishige Group, Tokyo, Japan)

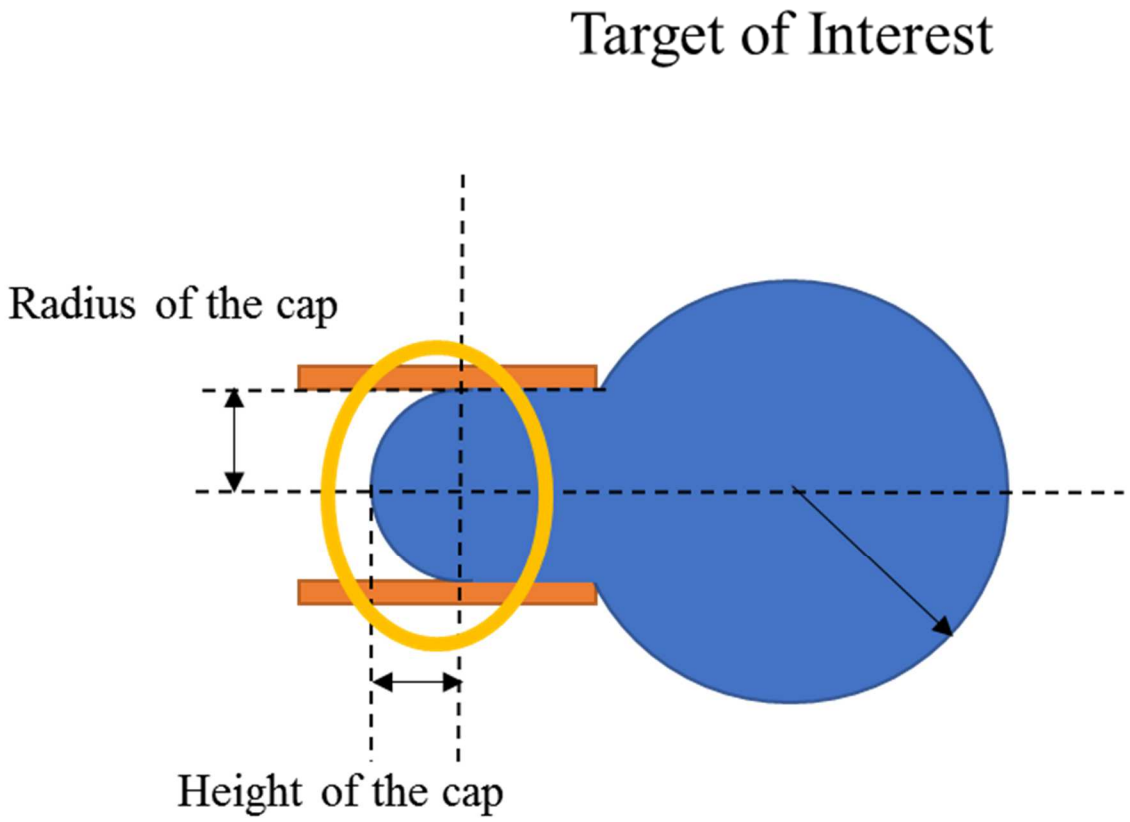

Figure 8: A schematic view of the target of interest: Only the hemispherical cap is studied to analyze for the stress distribution on the membrane.

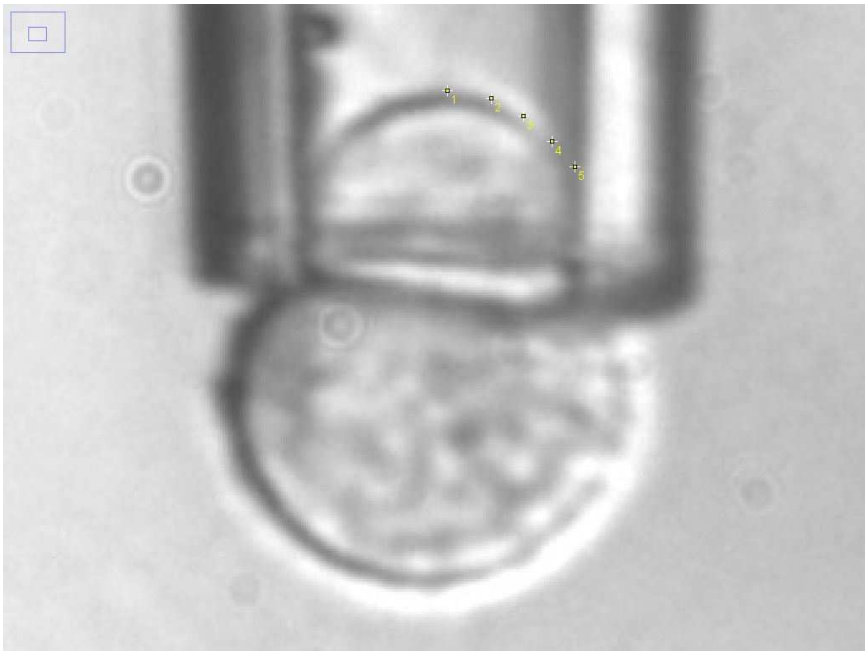

Figure 9: Discrete points used to capture the right half of cell membrane projection inside micropipette. These control points are later imported into Matlab to generate a curve that could be represented by a polynomial function.

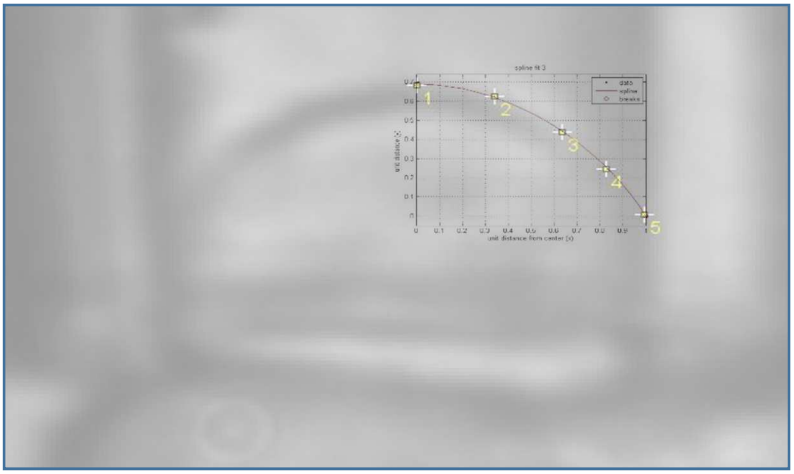

Figure 10: Figure overlapping the fitted curve with image data, representing the fitting quality.

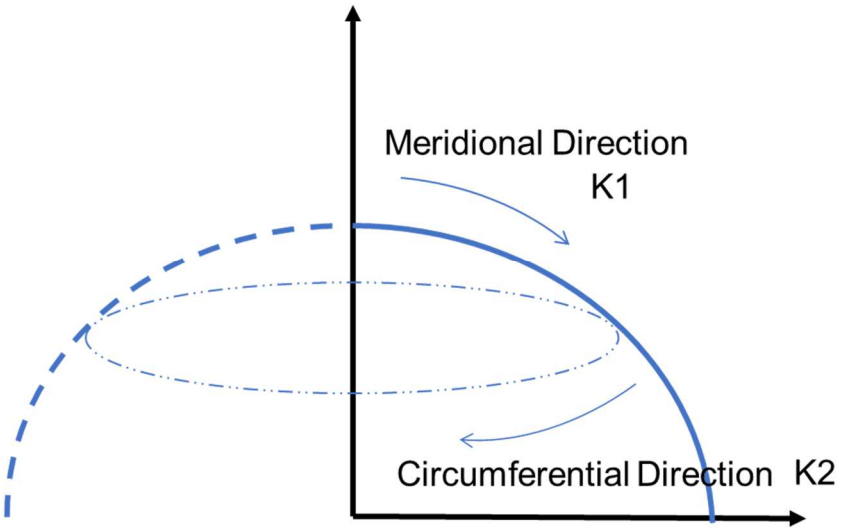

Figure 11: A schematic view of the tip of the membrane projection. This numerical calculation is based on a symmetric model, only the right half of the membrane is modeled. The curvatures on both meridional and circumferential direction are calculated and used to calculate principal stresses on both directions.

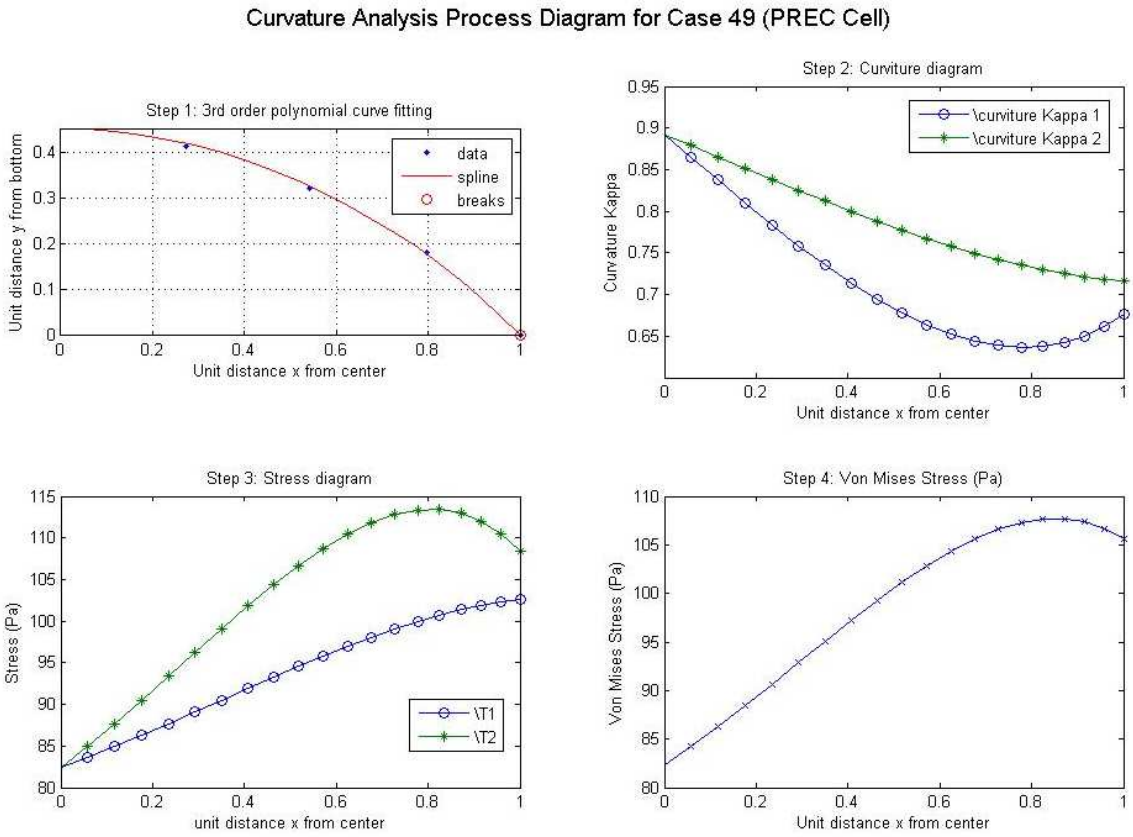

Figure 12: Example curvature analysis process diagram for case 49 (PrEC cell). Step 1: The process starts with a curve fitting using a 4th order polynomial function to trace the right half of the membrane from the control points collected from the source image. The horizontal axis represents the normalized distance from the center of the membrane. 0 accounts for the center of the membrane and 1 accounts for the membrane closer to the pipette wall. The starting point where x is equal to 0, is applied with constraint to limit the top part of the membrane completely flat and tangent to the horizontal axis to ensure a finite calculation. Step 2: The curve is then analyzed using two curvature equations to calculate curvature on both meridional (K1) and circumferential (K2) direction. It shows the largest curvature occurs at the beginning and lowest curvature occurs closer to the pipette wall where x is equal to 0.8. Step 3: From the curvature, two principal stress pointing towards both meridional (T1) and circumferential (T2) directions are calculated. The graph shows that the largest principal stress is also increased when the distance from the center of the membrane steps up. Step 4: Essentially principal stresses are used to generate von Mises stress curve. For this case, maximum stress is located closer the pipette walls where x is equal to 0.8.

CHAPTER 3: RESULTS

3.1 MAXIMUM RUPTURE PRESSURE AND RUPTURE RATE

From the previous experiment performed by Chivukula, it is observed that PC-3 cancer cells are easier to be aspirated into the micropipette tube compared to PrEC cells, which indicates a stiffer material property. At rest, Young's modulus of PrEC cell is about 130% stiffer than PC-3 cells (Chivukula et al., 2014). The result was supported by multiple studies using Atomic Force Microscopy and concluded that PrEC cells were over 80% stiffer than PC-3 cells.

The primary focus of the current study is to study the strength of both PC-3 and PrEC cell membranes. From the 57 cases collected, including 40 PC-3 cells and 17 PrEC cells, the minimum hydrostatic pressure required to cause PC-3 cells rupture is significantly lower than PrEC cells. Due to significantly longer cell preparation time for PrEC cells, we've studied less PrEC cell cases compared to PC-3 cells. From the distribution of normalized maximum rupture pressure histogram shown in Figure 13, we can see that PrEC cells are more likely to develop rupture when pressure is larger than 30 mmH2O, while PC-3 cells have a standard distribution ranged from 15 to 35 mmH2O. A normalized maximum rupture pressure histogram is also shown in Figure 14, allowing a closer comparison eliminating the population gap between two cell types. According to the maximum rupture pressure distribution diagram shown in Figure 15, the average rupture pressure for PC-3 cells is 32.13 mmH2O excluding an outlier which developed rupture at 45 mmH2O and the average for PrEC cells is 41.5 mmH2O. Also, Figure 16 compares the

rupture rate of both cell types and shown that PC-3 cells have a much more significant rupture rate of 75% compared to PrEC cells, which have 35.3% rupture rate within the 50 mmH2O hydrostatic pressure limit. In general, these statistical results represent that PrEC cells have larger resistance to the hydrostatic pressure and have more strength compared to PC-3 cells.

3.2 OBSERVATION FROM THE EXPERIMENT

One of the major observations from the current experiment could be responsible for the strength difference of the cell membranes. When the cell membrane was slowly aspirated into the pipette, the profile of the membrane inside gradually changed due to the increased pressure level, this behavior significantly separates PrEC cells and PC-3 cells. The PC-3 cell's membrane tends to flatten under pressure and will soon reaches its rupture point, losing its integrity. An example of this flatten behavior of PC-3 cell is shown in Figure 17 and the von Mises stress distribution diagram correspond to this cell is shown in Figure 18. This flattens shape generally caused by faster elongation of membrane parts that are closer to the pipette wall compare to the center. However, the PrEC cell's membrane retains its rounded geometry and tends to survive longer when the pressure increases. In some cases, the PrEC cells can even form more spherical shapes so that the center of the membrane parts elongated faster than the parts closer to the pipette wall, distributes the pressure evenly. An example of this round behavior of PrEC cell is shown in Figure 19 and the von Mises stress distribution diagram correspond to this cell is shown in Figure 20. Some results show an opposite behavior demonstrating infrequent cases are also shown (Figure 21-24). Some PC-3 cells occasionally retrieve to a more spherical shape and

maximum von Mises stress doesn't increase significantly compare to other PC-3 cells as a response, some PrEC cells become slightly flattened and its maximum von Mises stress increase significantly compare to other PrEC cells. The von Mises stress distribution results which reported higher von Mises stress closer to the pipette walls coincide with the observations from the experiments as most of the rupture points are located closer to the pipette walls. An example of a rupture PrEC cell is shown in Figure 25, the analysis for this case presents a high local von Mises stress closer to the pipette wall at 25 mmH2O and a rupture occurred at the predicted location at 30 mmH2O indicating cell failure.

3.3 RELATIONSHIP BETWEEN VON MISES STRESS AND SHAPE

The shape of the membrane significantly affects the von Mises stress distribution causing maximum stress differences between PC-3 and PrEC cells. For membranes that have a rounder and spherical shape, its stress is more uniformly distributed, and the maximum stress doesn't increase much for each gradient of hydrostatic pressure increment. However, for membranes that have a flattened shape, producing a higher stress closer to the pipette wall. This behavior directly affects the chance of cell failure. Laplace Law explains this result that when the membrane is a perfect hemispherical shape where in the curvature is consistent, the stress should also be uniformly distributed.

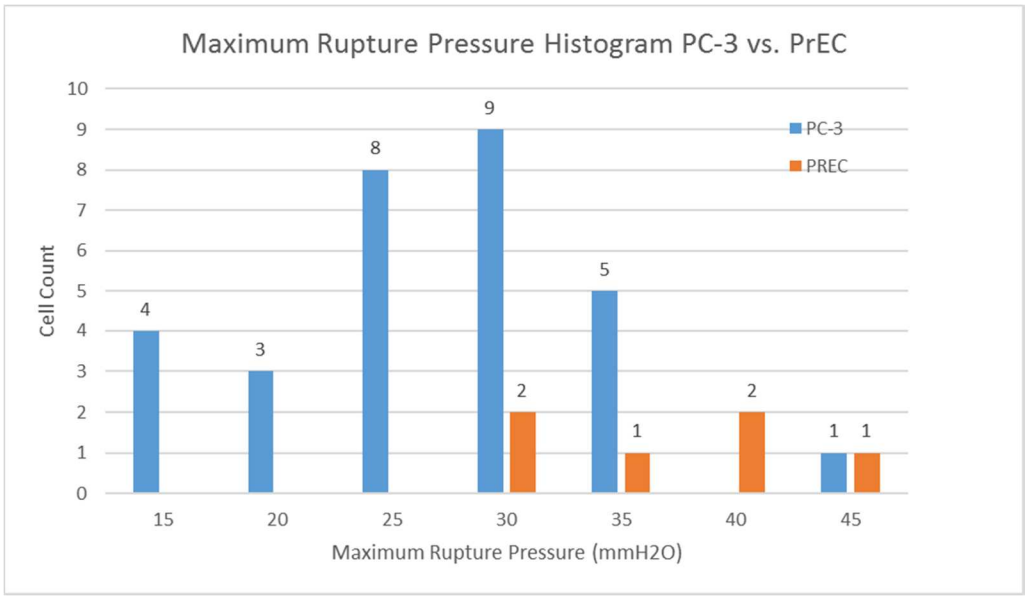

Figure 13: Maximum rupture pressure histogram for PC-3 cells and PrEC cells. PC-3 cells represent lower resistance to increasing pressure level compare to PrEC cells. In some cases, the minimum pressure requires causing PC-3 cells to rupture occurs as early as 15 mmH2O. Comparatively, PrEC cells did not present rupture characteristics until 30 mmH2O. The distribution of the data is also shown in a box and whisker plot for comparison and analysis.

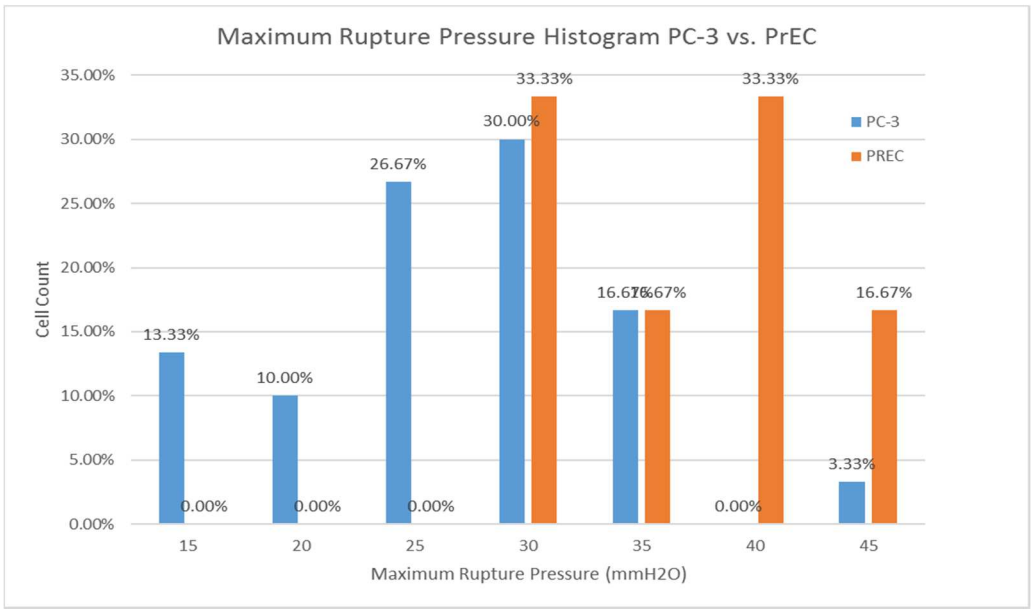

Figure 14: Normalized maximum rupture pressure histogram for PC-3 cells and PrEC cells.

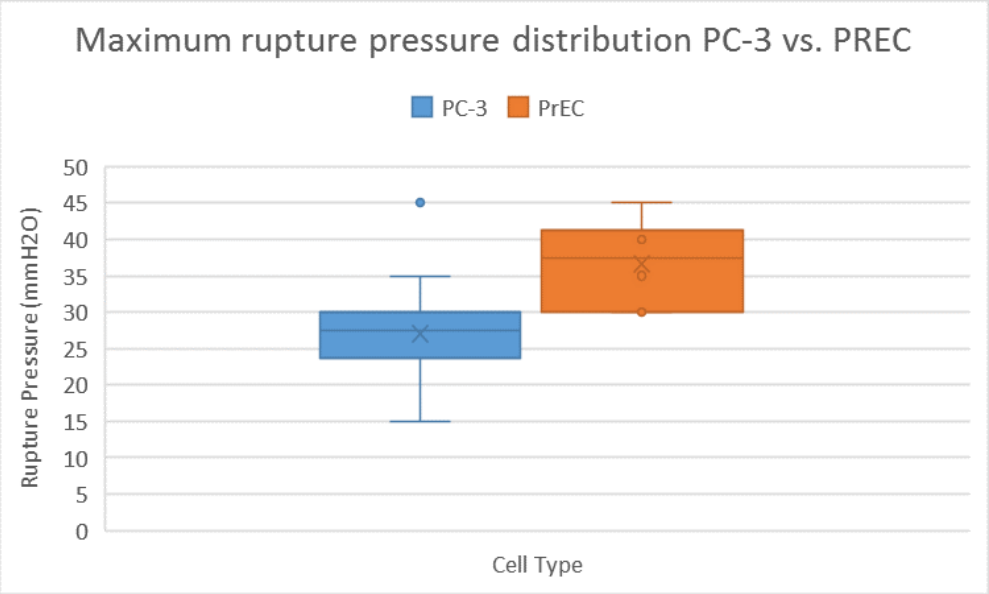

Figure 15: Maximum rupture pressure distribution PC-3 vs. PrEC. The average rupture pressure for PC-3 cells is 27 mmH2O while for PrEC cells is 36.67 mmH2O.

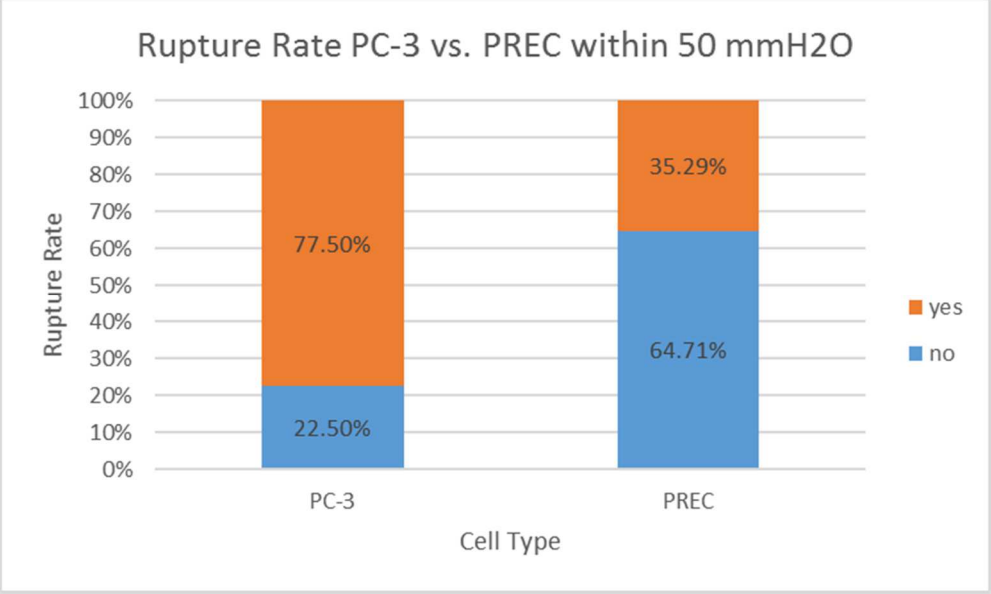

Figure 16: Rupture rate diagram for PC-3 cells and PrEC cells within 50 mmH2O. PC-3 cells present a 75 percent rupture rate, while PrEC cells only present a 35.3 percent rupture rate.

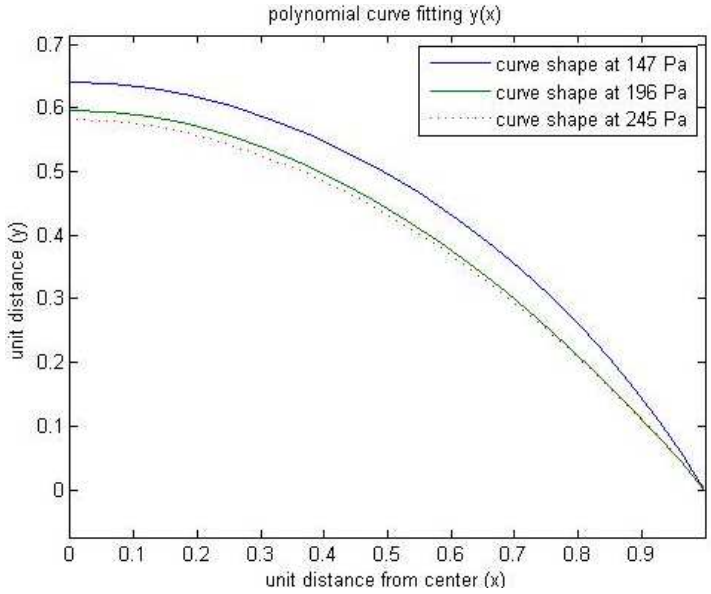

Figure 17: Polynomial curve fitting to represent the right half of a meridional cell membrane profile (PC-3 cell, Case 18) at three different pressure level. The unit was scaled into the unit distance for consistent comparison. This graph shows that the curve tends to become more flattened when pressure increases. Keep in mind that the flattening of the membrane is caused by a faster elongation of membrane closer to the pipette wall compare to the center, not shrinking after being aspirated.

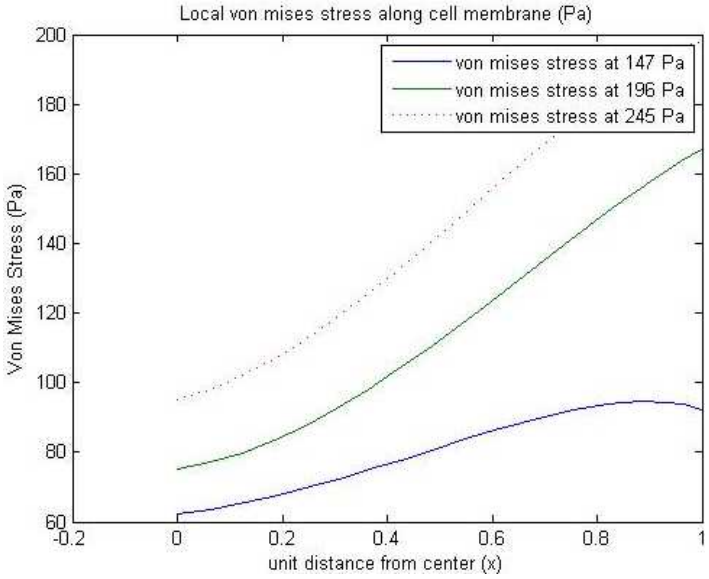

Figure 18: Von Mises stress along a half scaled axisymmetric cell membrane (PC-3 cell, Case 18) at three different pressure level. The slope of the stress curve increases when pressure increases, which result in high stress closer to the pipette wall.

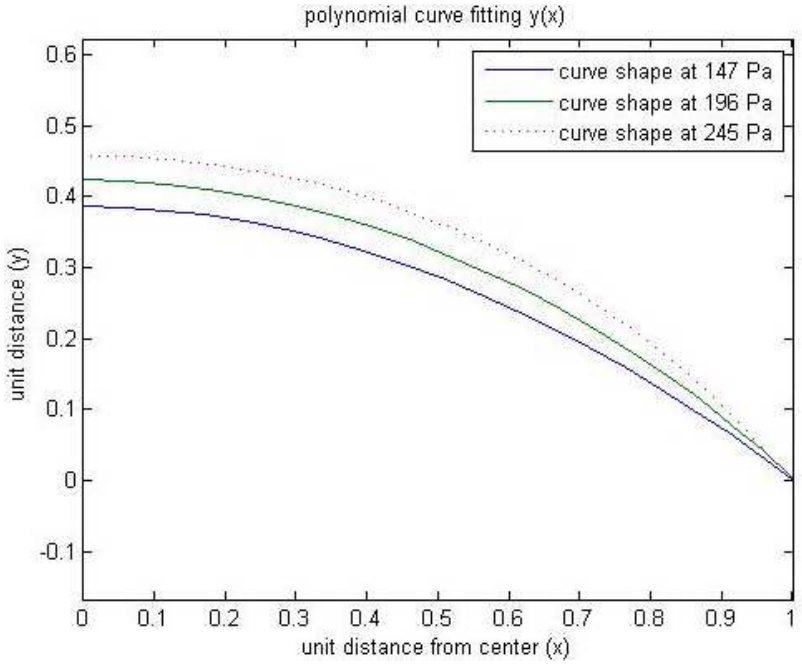

Figure 19: Polynomial curve fitting to represent the right half of a meridional cell membrane profile (PrEC cell, Case 54) at three different pressure level. The unit was scaled into the unit distance for consistent comparison.

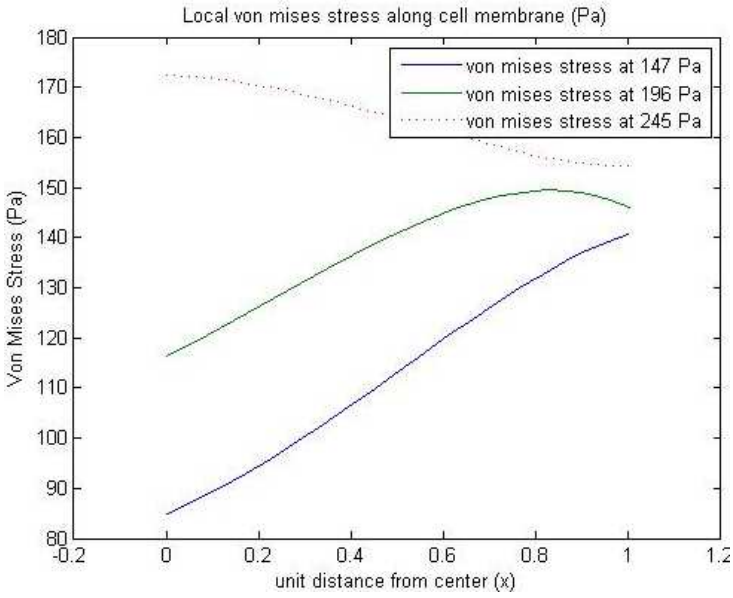

Figure 20: Von Mises stress along a half sized axisymmetric cell membrane (PrEC cell, Case 54) at three different pressure level. The trend of the stress curve is comparatively consistent throughout the membrane which allows an even force distribution. As a result, lower maximum stress.

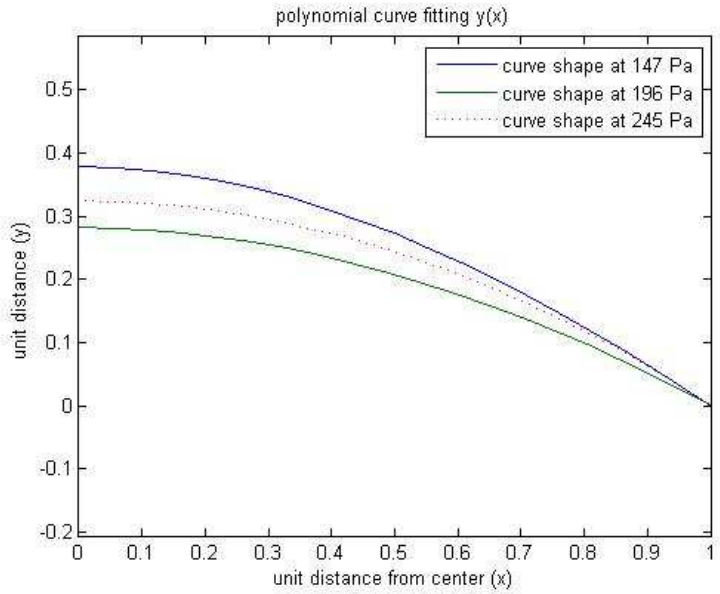

Figure 21: Polynomial curve fitting to represent the right half of a meridional cell membrane profile (PC-3 cell, Case 36) at three different pressure level. The unit was scaled into the unit distance for consistent comparison.

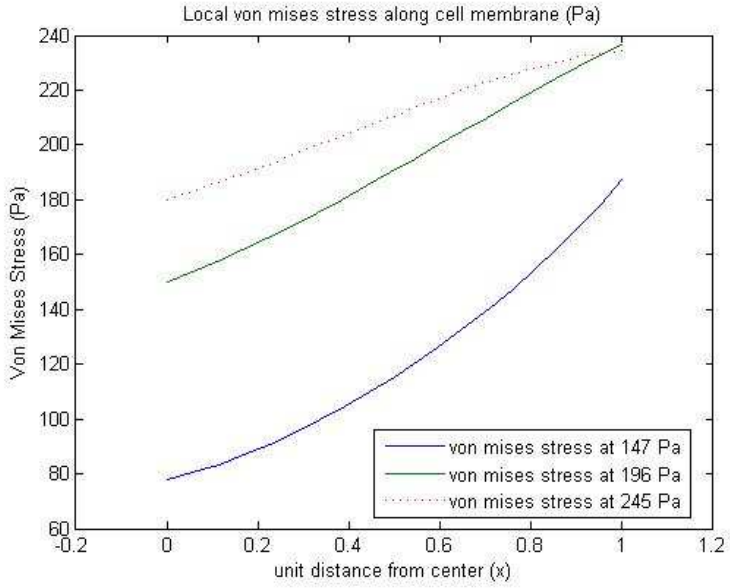

Figure 22: Von Mises stress along a half scaled axisymmetric cell membrane (PC-3 cell, Case 36) at three different pressure level. The trend of the stress curve at 245 Pa essentially become more flattened which result in similar maximum stress compare to stress at 196 Pa.

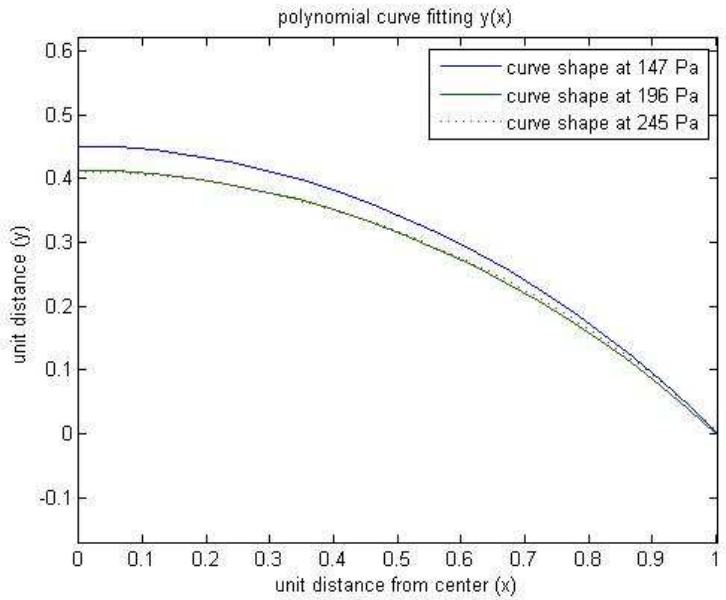

Figure 23: Polynomial curve fitting to represent the right half of a meridional cell membrane profile (PrEC cell, Case 49) at three different pressure level. The unit was scaled into the unit distance for consistent comparison.

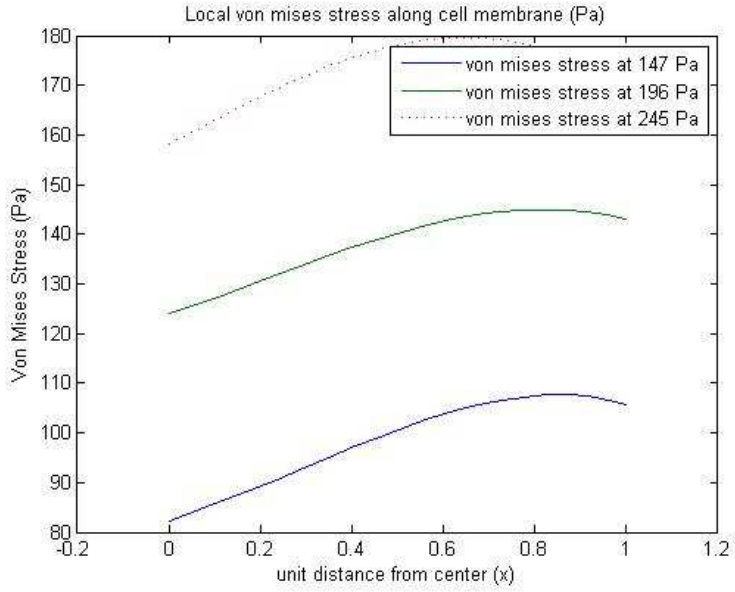

Figure 24: Von Mises stress along a half sized axisymmetric cell membrane (PrEC cell, Case 49) at three different pressure level. The shape of the curve does not differ much, so the trend of the stress curve is comparatively consistent which the relationship between the pressure and von Mises stress is linear.

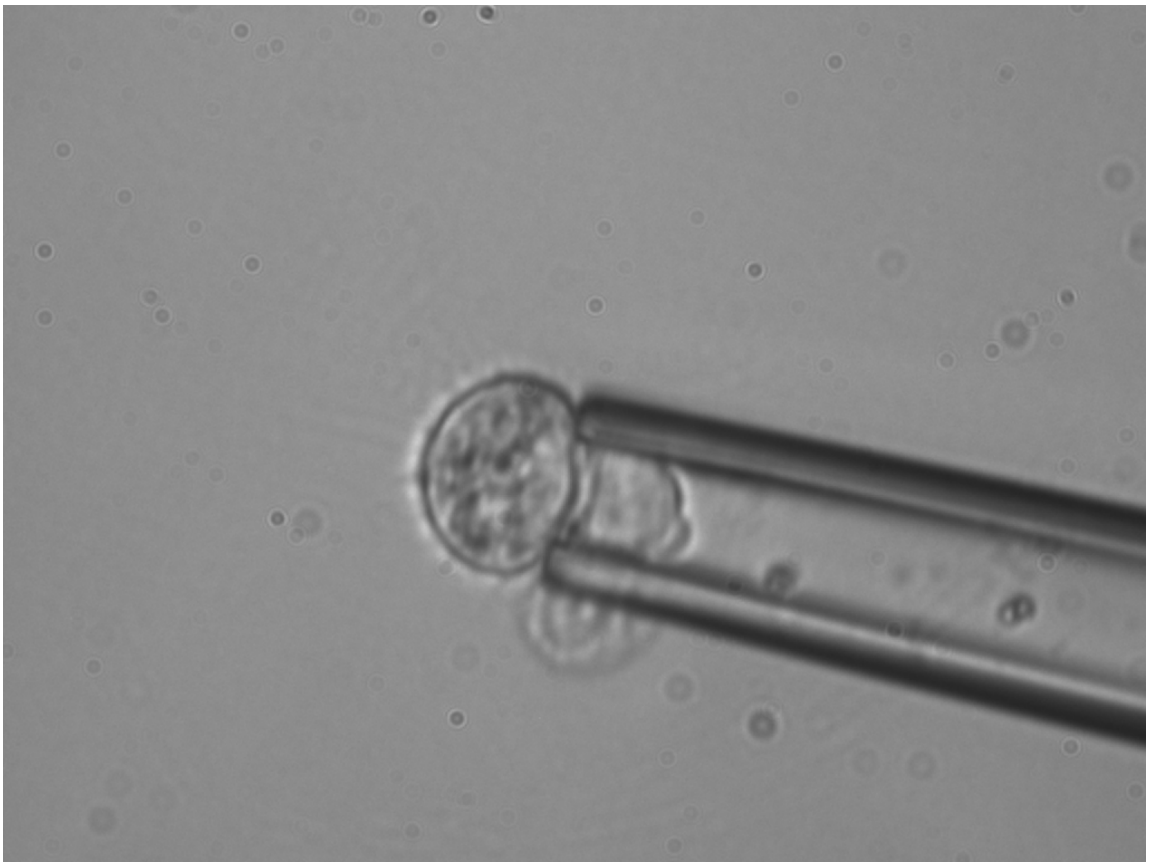

Figure 25: Rupture process of a sample PrEC cell (Case 49). The experimental result aligned with the curvature analysis. The location of the actual rupture point is located closer to the pipette wall, and our analysis shows that the maximum von Mises stress is also located close to the pipette wall.

CHAPTER 4: DISCUSSION

4.1 CONCLUSION

From the observation of the experiment and statistical results collected from all the cases combined with previous research works, it is adequate to conclude that PC-3 cells are easier to rupture compared to PrEC cells under aspiration pressure. When aspirated into the micropipette, PrEC cells retain a close-to spherical shape while PC-3 cells membrane tends to become more flattened. This means the membrane part closer to the pipette wall for a PC-3 cell is more aspirated compared to a PrEC cell. Their variation in shape when exposed to hydrostatic pressure increment significantly differs their local von Mises stress distribution. PrEC cells with spherical shape membrane show a more even stress distribution and have low maximum stress locally. PC-3 cells with flattened membranes show uneven stress distribution and have high maximum stress locally near the pipette wall. A comparison of both cells regarding von Mises stress is shown in Figure 26. PC-3 cells membrane exposed to larger von Mises stress locally compared to PrEC cells. By comparing the histogram shown in Figure 26 and the relationship between pressure and von Mises stress for PrEC cells in Figure 27 and PC-3 cells in Figure 28, the trend shows that the von Mises stress increment for PC-3 cells is higher than PrEC cells when pressure increases. Besides, these graph is only capturing pressure gradient from 147 Pa to 245 Pa where both cells have not yet reach their rupture point. We would predict that the PC-3 cells under higher gradient pressure level will generate more stress on the local membrane and eventually leads to a quick reach of rupture point and high rupture rate. By comparing

histograms of maximum von Mises stress under three pressure level (Figure 29-31), PrEC cells show a significant lower frequency overall compare to PC-3 cells and this appearance becomes more significant in higher pressure level (245 Pa). From the stress range diagram shown in Figure 32, PC-3 cells have significantly large stress range compared with PrEC cells, which we believe is majorly responsible for the high-stress located on the side closer to the pipette wall. Our experimental observation also supports this result that most rupture occurs on the side of the inflated membrane closer to the pipette wall.

4.2 EXPERIMENT PROTOCOL UPDATE

Although existing protocols cover the basic operations, there are still rooms for better research design in the future. The first suggestion is to exchange micropipette after three times of experiment or proper measurement of aspiration pressure on the tip. Usually, after using a pipette for a certain amount of time, ruptured cell membrane residues could attach to the pipette rim causing toroidal rim inefficient at aspirating cells and may create leakage. Dead cell membrane wrapped around both the inner wall and outer periphery of the pipette could also decrease the image quality while also affect the result of the next aspirated cell. The experiment length for one batch of the cell prepared needs to be performed within an hour. Multiple experiments have shown that when the operation time extent for over an hour, more cell death appears, and there are studies have indicated that dying cells tend to stiffen themselves and this will interrupt with the material failure study.

The second recommendation is to time the exposure of the hydrostatic pressure accurately. The consistency of time between each gradient of pressure increment could significantly change the result. It is important to record it as this could differ from an

experiment of cells getting exposure to stress or an experiment of cells in steady state briefly and reaching force equilibrium. To better define the target of interest which is the cap of the membrane projection inside pipette wall, Lp/Rp is also preferably to be recorded to determine if the aspiration time is consistent. Previous researchers have found that there is a linear relationship between Lp/Rp and pressure increment.

Third, a better way of determining if the cell is reaching its rupture point is also necessary to make a well-founded judgment. The current way to determine the rupture is to measure the area of the cell since the area of the cell should stay the same before the rupture even though the micropipette slightly alters the shape. When the cell reaches its rupture point, a loss in membrane integrity and an increase in total cell area is expected. We could potentially use fluorescent dye to mark the cell membrane and detect the exact rupture point to draw a better conclusion. Fluorescent dye could also upgrade the experiment to a different level by marking important elements inside membrane such as nucleus and cytoplasm which could affect the Lp/Rp where in some rare cases nucleus could stuck cells from being aspirated into micropipettes. The cell dis significantly changed with the progress of cell death and is very susceptible to mechanical cell damage (Nikolaev, Müller, Williams, & Liu, 2014). Because of that, there exists necessity to detect cell's healthiness through the fluorescent microscopic method and carefully control the cell exposure time under a microscope to avoid cell death and ensure an accurate result.

4.3 ASSUMPTION JUSTIFY

The numerical model and calculation could be improved by adding additional assumptions such as making the end of the curve tangent to the pipette wall as we did for

the top of the membrane. This could help us form curves that are better capturing the overall shape of the membrane. However, this improvement wouldn't change our overall results since the PC-3 cells have less curvature overall compare to PrEC cells, and the numerical model calculation is independent as the in-plane stress is calculated directly from the curvature locally.

4.4 SUMMARY AND FUTURE WORKS

From the observation of micro pipette aspiration experiment and geometric stress analysis of cell membrane, the results indicate that non-transformed prostate epithelial cells (PrEC LH) exhibited a higher rupture strength compared with transformed prostate cancer cells (PC-3). When the pressure inside the micropipette loads cells, cancer cells are reformed into a more flattened shape, causing stress distributed unevenly and easily lost its integrity. In contrast, normal PrEC cells tend to retain its rounded shape, causing stress distributed more evenly along the membrane and able to sustain more pressure. At higher pressures, the PrEC cells tend to have a spherical shape, leading to a uniform tension distribution. This could indicate cancer cells may have different structural parameters of the cytoskeleton, including total fiber- associated fluorescence, as well as fiber length and orientation (Lichtenstein, Geiger, & Kam, 2003). Cancer cell are also immature so that they have lower resistance to pressure or a unique cellular response or different microstructure on cancer cells as a response to mechanical stimuli. Multiple pieces of research have shown a larger stiffness of healthy cells compared with cancer cells and one of the recent studies found that cancer cell tends to become stiffer after exposing to fluid shear stress. We are

curious to see if the fluid shear stress could also affect cells' rupture property and overall survivability using this method.

Although extensive research and experiment are necessary to make a definite conclusion, this result may provide significant insights to a geometric relationship between membrane and stress and developing a new quantitative method to measure maximum failure stress and local stress distribution of cell membrane. The novel discovery of this cellular behavior could support the area of studying cancer cell membrane structural parameters of the cytoskeleton, including total fiber-associated fluorescence, as well as fiber length and orientation (Lichtenstein N, July 2003), response to mechanical loadings and potentially aid in cancer treatment development other than destructive chemical treatment. This numerical analysis method we invented is also readily applicable and transferable to another cellular type of studies regarding cell's mechanical properties.

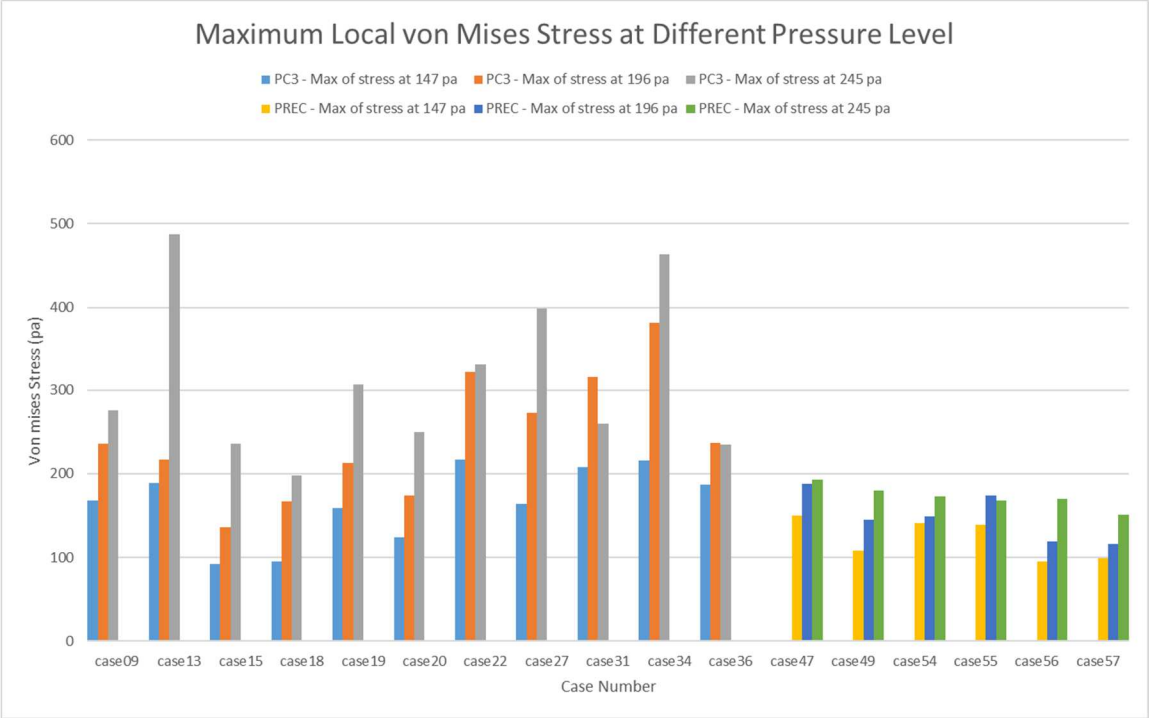

Figure 26: Maximum von Mises stress at different pressure level for PC-3 cells and PrEC cells. This graph separates into two groups, PC-3 cells on the left and PrEC cells on the right. For each case, three bars representing maximum local stress on cell membrane at three incremental pressure level. The major observation from the graph is that while the pressure level is increasing, the maximum stress of PrEC cells does not increase as much as PC-3 cells do.

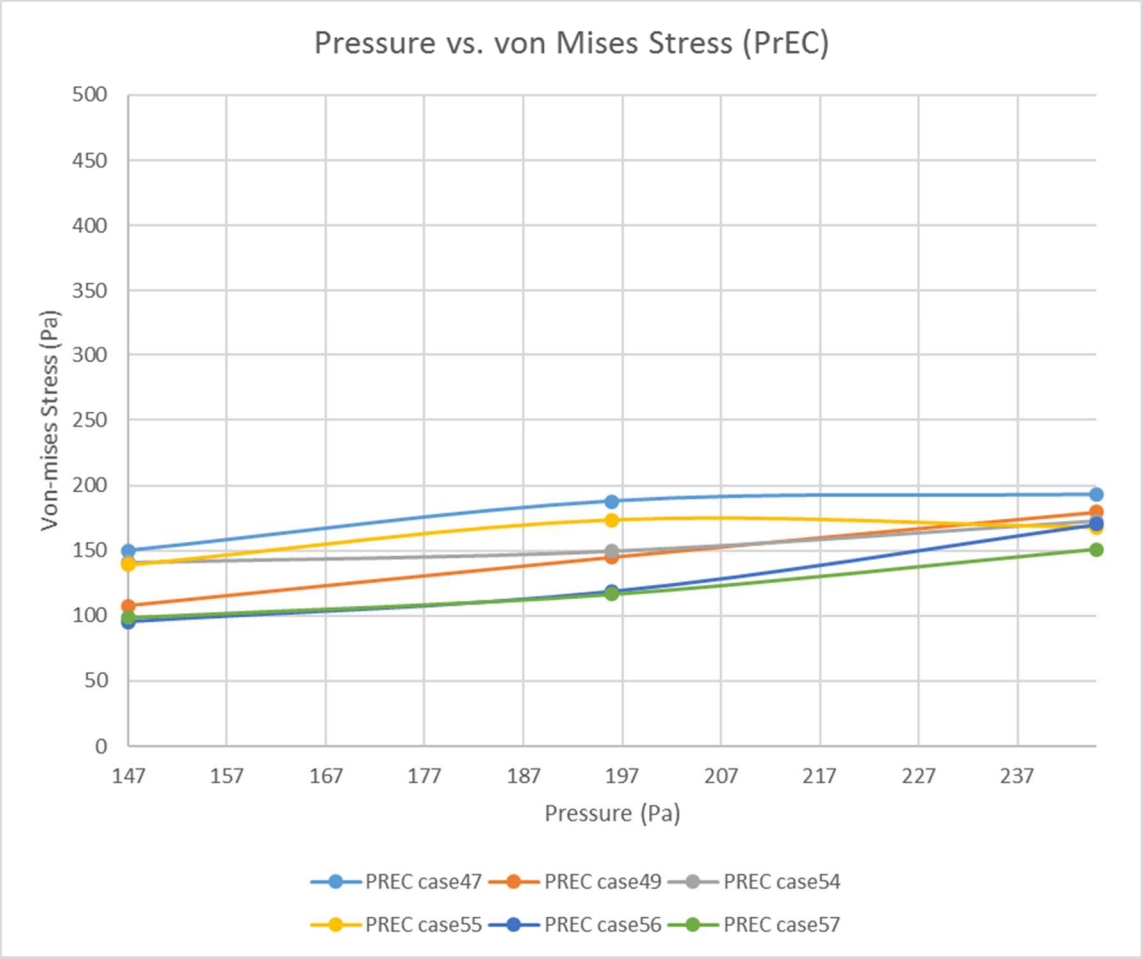

Figure 27: The pressure vs. von Mises stress diagram for each specific cases for PrEC cells. The local von Mises stress gradually increases when the pressure increases. Comparatively, this increment is not significant compared to PC-3 cells.

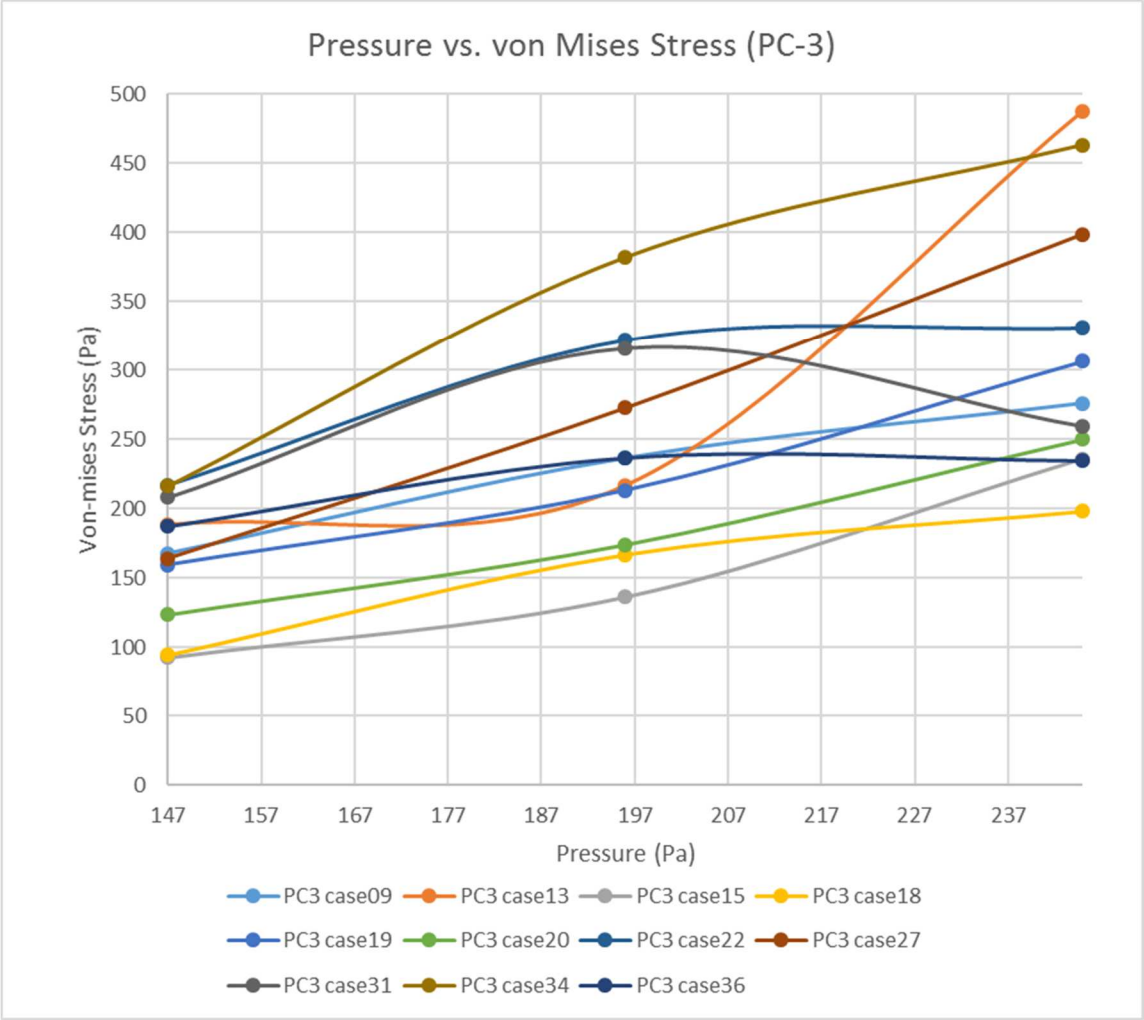

Figure 28: The pressure vs. von Mises stress diagram for each specific cases for PC-3 cells. The local von Mises stress increases dramatically when the pressure increases. Comparatively, this increment is significant compared to PC-3 cells where the trend is almost exponential in some cases.

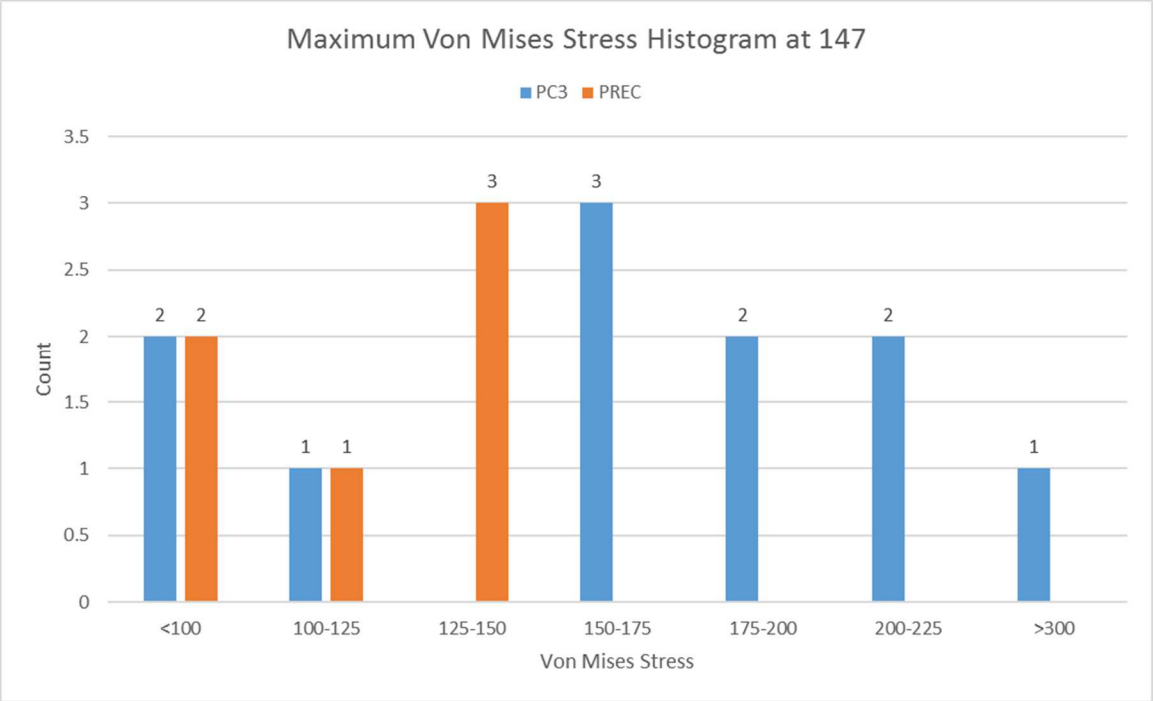

Figure 29: Maximum Von Mises Stress on cell membrane when pressure is 147 Pa.

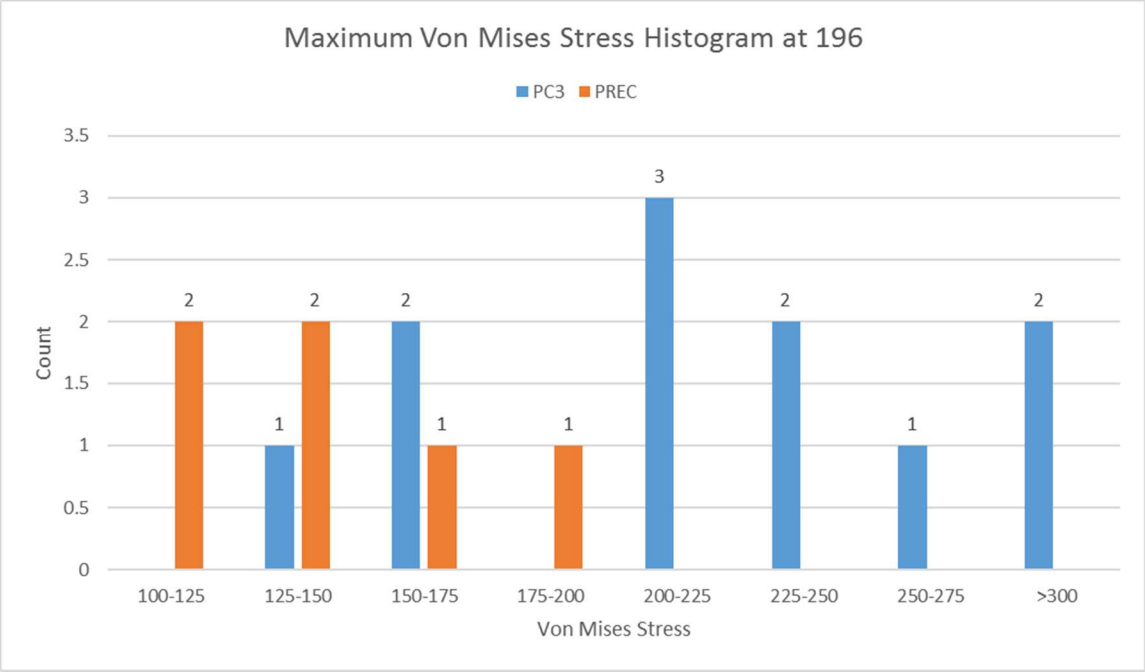

Figure 30: Maximum Von Mises Stress on cell membrane when pressure is 196 Pa.

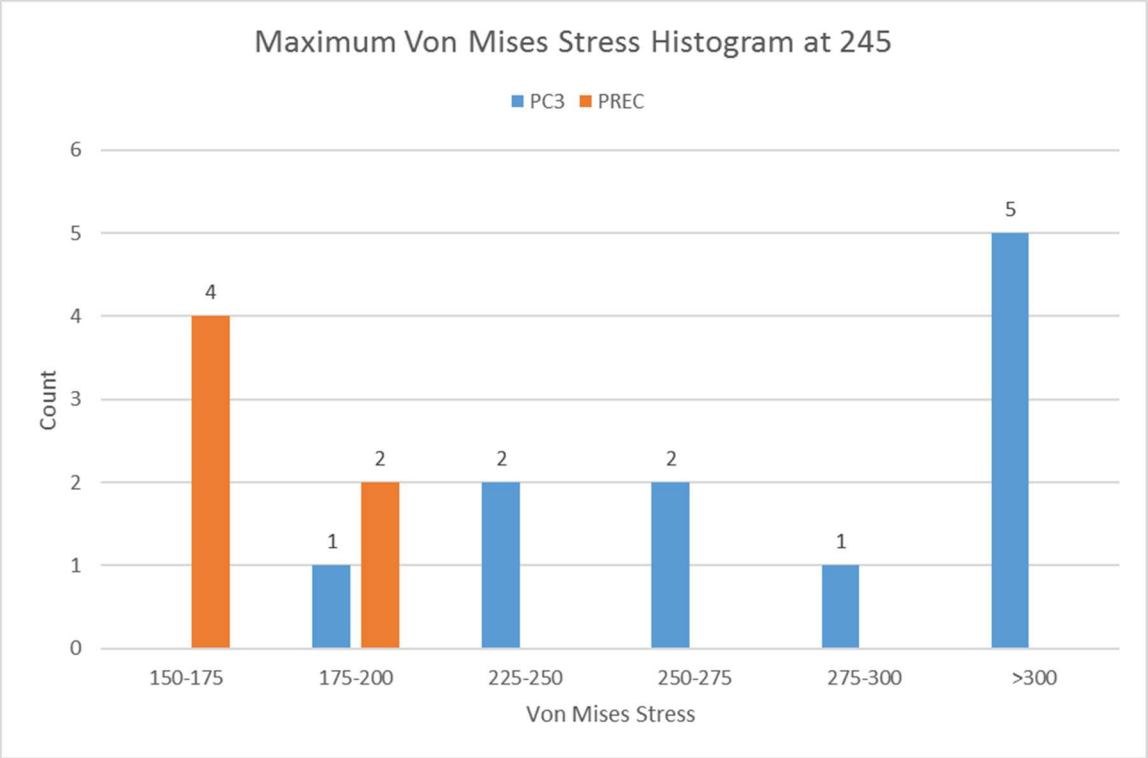

Figure 31: Maximum Von Mises Stress on cell membrane when pressure is 245 Pa.

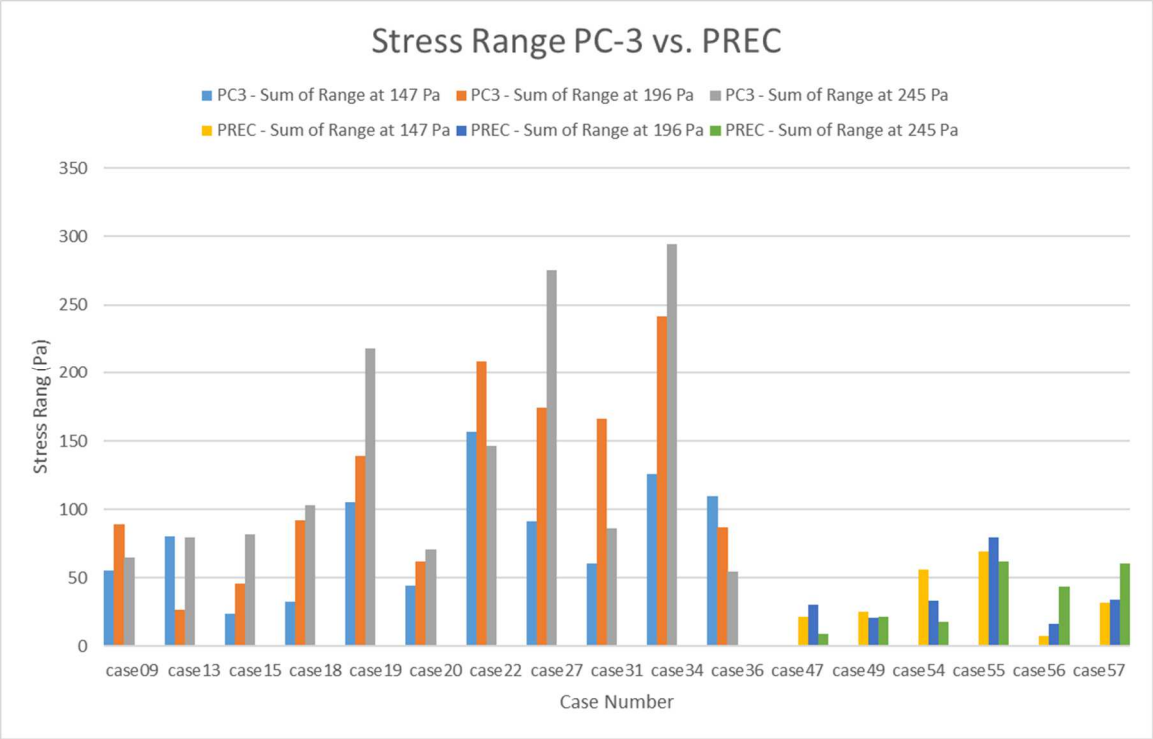

Figure 32: Stress Range at different pressure level for PC-3 cells and PrEC cells. Stress range is calculated from the difference of maximum and minimum stress. The graph shows that the stress range is relatively small for PrEC cells compare to PC-3 cells. This represents that the stress on PrEC cell membrane is more evenly distributed than PC-3 cells which could result in low maximum stress.

BIBLIOGRAPHY

Barnes, J. M., Nauseef, J. T., & Henry, M. D. (2012). Resistance to Fluid Shear Stress Is a Conserved Biophysical Property of Malignant Cells. PLOS ONE, 7(12), e50973. https://doi.org/10.1371/journal.pone.0050973

Chivukula, V. K., Chivukula, V. K., & Lu, J. (2014). Development of a Nurbs-Based Particulate Dynamics Framework for Modeling Circulating Cells.

Chivukula, V. K., Krog, B. L., Nauseef, J. T., Henry, M. D., & Vigmostad, S. C. (2015). Alterations in cancer cell mechanical properties after fluid shear stress exposure: a micropipette aspiration study. Cell Health and Cytoskeleton, 7, 25–35. https://doi.org/10.2147/CHC.S71852

Evans, E., Skarlek, R., & Weinbaumu, S. (1980). Mechanics and Thermodynamics of Biomembranes. Journal of Biomechanical Engineering.

Gossett, D. R., Tse, H. T. K., Lee, S. A., Ying, Y., Lindgren, A. G., Yang, O. O., … Di Carlo, D. (2012). Hydrodynamic stretching of single cells for large population mechanical phenotyping. Proceedings of the National Academy of Sciences of the United States of America, 109(20), 7630–7635. https://doi.org/10.1073/pnas.1200107109

Guck, J., Schinkinger, S., Lincoln, B., Wottawah, F., Ebert, S., Romeyke, M., … Bilby, C. (2005). Optical deformability as an inherent cell marker for testing malignant transformation and metastatic competence. Biophysical Journal, 88(5), 3689–3698. https://doi.org/10.1529/biophysj.104.045476

Gupta, G. P., & Massagué, J. (2006). Cancer Metastasis: Building a Framework. Cell, 127(4), 679–695. https://doi.org/10.1016/j.cell.2006.11.001

Hochmuth, R. M. (2000). Micropipette aspiration of living cells. Journal of Biomechanics, 33(1), 15–22.

Kreysing, M. K., Kiessling, T., Fritsch, A., Dietrich, C., Guck, J. R., & Käs, J. A. (2008). The optical cell rotator. Optics Express, 16(21), 16984–16992.

Lekka, M., Laidler, P., Gil, D., Lekki, J., Stachura, Z., & Hrynkiewicz, A. Z. (1999). Elasticity of normal and cancerous human bladder cells studied by scanning force microscopy. European Biophysics Journal: EBJ, 28(4), 312–316.

Lulevich, V., Zink, T., Chen, H.-Y., Liu, F.-T., & Liu, G.-Y. (2006). Cell mechanics using atomic force microscopy-based single-cell compression. Langmuir: The ACS Journal of Surfaces and Colloids, 22(19), 8151–8155. https://doi.org/10.1021/la060561p

Luzzi, K. J., MacDonald, I. C., Schmidt, E. E., Kerkvliet, N., Morris, V. L., Chambers, A. F., & Groom, A. C. (1998). Multistep Nature of Metastatic Inefficiency. The American Journal of Pathology, 153(3), 865–873.

Mehlen, P., & Puisieux, A. (2006). Metastasis: a question of life or death. Nature Reviews Cancer, 6(6), 449–458. https://doi.org/10.1038/nrc1886

Nikolaev, N. I., Müller, T., Williams, D. J., & Liu, Y. (2014). Changes in the stiffness of human mesenchymal stem cells with the progress of cell death as measured by atomic force microscopy. Journal of Biomechanics, 47(3), 625–630. https://doi.org/10.1016/j.jbiomech.2013.12.004

Siegel, R. L., Miller, K. D., & Jemal, A. (2016). Cancer statistics, 2016. CA: A Cancer Journal for Clinicians, 66(1), 7–30. https://doi.org/10.3322/caac.21332

Suresh, S. (2007). Biomechanics and biophysics of cancer cells. Acta Biomaterialia, 3(4), 413–438. https://doi.org/10.1016/j.actbio.2007.04.002

Theret, D. P., Levesque, M. J., Sato, M., Nerem, R. M., & Wheeler, L. T. (1988). The Application of a Homogeneous Half-Space Model in the Analysis of Endothelial Cell Micropipette Measurements. Journal of Biomechanical Engineering, 110(3), 190–199. https://doi.org/10.1115/1.3108430

Weiss, L., Dimitrov, D. S., & Angelova, M. (1985). The hemodynamic destruction of intravascular cancer cells in relation to myocardial metastasis. Proceedings of the National Academy of Sciences of the United States of America, 82(17), 5737–5741.

Wirtz, D., Konstantopoulos, K., & Searson, P. C. (2011). The physics of cancer: the role of physical interactions and mechanical forces in metastasis. Nature Reviews Cancer, 11(7), 512–522. https://doi.org/10.1038/nrc3080

MATLAB R2014a, The MathWorks, Inc., Natick, Massachusetts, United States.

Lundgren, Jonas (2017). SPLINEFIT, MATLAB Central File Exchange. Retrieved May 1,2017.